Finite element structural response sensitivity and reliability analyses using smooth versus non-smooth material constitutive models

Michele Barbato and Joel P. Conte*

Department of Structural Engineering,
University of California,
San Diego, 9500 Gilman Drive,
La Jolla, CA 92093, USA
E-mail: mbarbato@ucsd.edu
E-mail: jpconte@ucsd.edu
*Corresponding author

Abstract: This paper focuses on the effects upon the design point search of gradient discontinuities caused by non-smoothness of material constitutive models in the context of finite element reliability analysis. The response computation algorithm for the Menegotto-Pinto smooth material constitutive model is extended to response sensitivity analysis using the Direct Differentiation Method. Response sensitivity and reliability analysis results are compared for a structural system modelled using smooth and non-smooth material constitutive laws, respectively. Both material and discrete loading sensitivity parameters are considered. Structural reliability analyses are performed using the First-Order Reliability Method. Implications of using smooth versus non-smooth material constitutive models in finite element response, response sensitivity and reliability analyses are discussed. A sufficient condition on the smoothness of uni-axial material constitutive models for obtaining continuous finite element response sensitivities is stated and proved for the quasi-static case. The issue of continuity/discontinuity of response sensitivities for the dynamic case is discussed within the application examples.

Keywords: material constitutive models; material constitutive parameters; finite element sensitivity analysis; gradient-based optimisation methods; structural reliability analysis.

Reference to this paper should be made as follows: Barbato, M. and Conte, J.P. (2006) 'Finite element structural response sensitivity and reliability analyses using smooth versus non-smooth material constitutive models', *Int. J. Reliability and Safety*, Vol. 1, Nos. 1/2, pp.3–39.

Biographical notes: Michele Barbato is a graduate student researcher in the Department of Structural Engineering at the University of California, San Diego, USA. He received his Laurea (2002) in Civil Engineering from the University 'La Sapienza', Rome, Italy, and his MS (2005) in Structural Engineering at the University of California, San Diego. His current and past research activities are in the areas of finite element sensitivity and reliability analyses, earthquake engineering, modelling and analysis of R/C, steel and steel-concrete composite structures and FRP retrofits of R/C structures.

Joel P. Conte is a Professor and Vice Chair of the Department of Structural Engineering at the University of California, San Diego, USA. He received his Civil Engineering Diploma from the Swiss Federal Institute of Technology in Lausanne, Switzerland, in 1985 and his MS (1986) and PhD (1990) in Civil Engineering from the University of California, Berkeley, USA. He is a member of the American Society of Civil Engineers (ASCE), Earthquake Engineering Research Institute (EERI), Consortium of Universities for Research in Earthquake Engineering (CUREE), Pacific Earthquake Engineering Research Center (PEER), Network for Earthquake Engineering Simulation (NEES) and International Association for Structural Safety and Reliability (IASSAR). His research interests include modelling, analysis, identification and control of structures, earthquake engineering, structural reliability and risk analysis. He has published over 80 journal and conference publications. He is an Associate Editor of the ASCE *Journal of Engineering Mechanics* and a member of the Editorial Board of the *International Journal of Reliability and Safety*.

1 Introduction

The field of structural reliability analysis has seen significant advances in the last two decades (Ditlevsen and Madsen, 1996). Analytical and numerical methodologies have been developed and improved for the probabilistic analysis of real structures characterised in general by non-linear behaviour, material and geometric uncertainties and subjected to stochastic loads (Schueller et al., 2004). Reliability analysis methods have been successfully applied to such problems, as the ones encountered in civil engineering and typically analysed deterministically through the Finite Element Method (FEM) (Der Kiureghian and Ke, 1988).

Several reliability analysis methods, such as asymptotic methods (First- and Second-Order Reliability Methods) (Breitung, 1984; Der Kiureghian, 1996; Der Kiureghian and Liu, 1986; Der Kiureghian et al., 1987; Ditlevsen and Madsen, 1996) and importance sampling with sampling distribution centred on the design point(s) (Au and Beck, 2001a; Au et al., 1999; Melchers, 1989; Schueller and Stix, 1987) are characterised by the crucial step of finding the design point(s). In particular, asymptotic methods can provide reliability analysis results with a relatively small number of simulations (often of the order of 10–100 simulations for First-Order Reliability Method (FORM) analysis) and with a computational effort practically independent of the magnitude of the failure probability. Furthermore, these methods provide important information such as reliability sensitivity measures, as byproduct of the design point search (Hohenbichler and Rackwitz, 1986). Other reliability analysis methods, for example, subset simulation (Au and Beck, 2001b, 2003) and importance sampling with sampling distribution not centred at the design point(s) (Au and Beck, 1999; Ang et al., 1992; Bucher, 1988), do not use the concept of design point, do not require computation of response sensitivities, and therefore are not affected by smoothness or non-smoothness of the material constitutive models used. In general, the computational cost of these methods increases for decreasing magnitude of the failure probability. Thus, for very low failure probabilities, these methods could require a very large number of simulations.

In general, the design point(s) is(are) found as the solution(s) of a constrained optimisation problem, in which the number of variables corresponds to the number of

material, geometric and loading parameters modelled as random variables (Ditlevsen and Madsen, 1996). The most effective optimisation algorithms for high-dimensional problems are gradient-based methods coupled with algorithms for efficient and precise computation of response sensitivities to material, geometric and loading parameters (Liu and Der Kiureghian, 1991). Moreover, these methods assume some smoothness properties of the objective and constraint functions, on which the convergence properties are dependent. Constraint function(s) that arise in structural engineering problems often do not possess second-order differentiability, as required by gradient-based optimisation methods to achieve quadratic convergence rates (Gill et al., 1981). In general, they present discontinuities in the first derivatives (e.g. J_2 plasticity model, contact problems) or even in the response (e.g. crack propagation), and further discontinuities are introduced by numerical solution methodologies (e.g. finite element, finite difference, numerical integration).

Significant research efforts have been devoted to the development of smooth non-linear material constitutive models, to better describe actual material behaviour. Important characteristics such as Baushinger's effect for steel and hysteresis loops for concrete are most accurately described by smooth material models. Other smooth versus non-smooth material behavioural properties (e.g. shape of $\sigma - \varepsilon$ relation for concrete in tension) may have a negligible effect on simulated structural response, but a significant effect on response sensitivities to material parameters.

This paper describes some features of response sensitivity analysis using smooth and non-smooth material constitutive laws. The response sensitivity computation algorithm is presented for the Menegotto–Pinto (M–P) smooth constitutive model typically used for structural steel (Menegotto and Pinto, 1973). Continuity of finite element response sensitivities is analysed and a sufficient condition on the smoothness properties of material constitutive models to obtain such continuity is stated and proved for the quasi-static case. On the basis of application examples, remarks are made on the continuity (or lack thereof) of response sensitivities for the dynamic case, which is more difficult to study mathematically. Focus is on the effects upon the design point search of gradient discontinuities produced by non-smoothness of material constitutive models. The FORM (Ditlevsen and Madsen, 1996) is applied to reliability analysis of a structural system modelled with smooth and non-smooth material constitutive laws, respectively. Both probabilistic quasi-static pushover and dynamic analyses are considered. The Direct Differentiation Method (DDM) (Conte, 2001; Conte et al., 2003; Kleiber et al., 1997; Zhang and Der Kiureghian, 1993) is used for finite element response sensitivity analysis. The implications of using smooth versus non-smooth material constitutive models on finite element response and response sensitivity analyses as well as on reliability analysis are discussed. On the basis of the results obtained, conclusions are drawn on the need to use existing or develop new inelastic material constitutive models with specified smoothness properties both in the monotonic as well as cyclic hysteretic behaviour for applications requiring continuous response sensitivities such as gradient-based optimisation.

It is worth mentioning that response sensitivity analysis finds application not only in reliability analysis, which is the focus of this paper, but also in structural optimisation, structural identification and finite element model updating and any other field in which gradient-based optimisation techniques are used. The results presented in this paper are general and apply to any situation for which response sensitivity analysis is required.

2 Finite element reliability analysis and design point search

In general, the structural reliability problem consists of computing the probability of failure P_f of a given structure, which is defined as the probability of exceedance of some limit-state (or damage-state) function(s) when the loading(s) and/or structural properties and/or parameters in the limit-state functions are uncertain quantities modelled as random variables.

This paper focuses on component reliability analysis, that is, we consider a single limit-state function $g = g(\mathbf{r}, \boldsymbol{\theta})$, where $\mathbf{r}$ denotes a vector of response quantities of interest and $\boldsymbol{\theta}$ is the vector of random variables considered. The limit-state function g is chosen such that $g \leq 0$ defines the failure domain/region. Thus, the time-invariant component reliability problem takes the following mathematical form

$$P_f = P[g(\mathbf{r}, \boldsymbol{\theta}) \leq 0] = \int_{g(\mathbf{r}, \boldsymbol{\theta}) \leq 0} p_{\boldsymbol{\Theta}}(\boldsymbol{\theta}) \mathrm{d}\boldsymbol{\theta} \tag{1}$$

where $p_{\boldsymbol{\Theta}}(\boldsymbol{\theta})$ denotes the joint Probability Density Function (PDF) of random variables $\boldsymbol{\theta}$.

Moreover, it is assumed that the limit-state function describes a first-excursion problem in one of the following simple forms:

$$g = \begin{cases} u_{\lim} - u(\boldsymbol{\theta}, \overline{t}); & \text{(up-crossing problem)} \\ u(\boldsymbol{\theta}, \overline{t}) - u_{\lim}; & \text{(down-crossing problem)} \\ u_{\lim} - \left| u(\boldsymbol{\theta}, \overline{t}) \right|, \quad (u_{\lim} > 0); & \text{(double-barrier crossing problem)} \end{cases} \tag{2}$$

in which $u(\boldsymbol{\theta}, \overline{t})$ is a scalar displacement response quantity (i.e. nodal displacement) computed at $t = \overline{t}$, where t is an ordering parameter (loading factor in a quasi-static analysis or time in a dynamic analysis), $\overline{t}$ is a specified value of t (e.g. $\overline{t} = \max(t)$ in a pushover analysis) and $u_{\lim}$ is a deterministic threshold. In this case, the time-invariant reliability problem reduces to computing

$$P_f = P\left[g(\boldsymbol{\theta}, \overline{t}) \leq 0 \right] = \begin{cases} P\left[u(\boldsymbol{\theta}, \overline{t}) \geq u_{\lim} \right] \\ P\left[u(\boldsymbol{\theta}, \overline{t}) \leq u_{\lim} \right] \\ P\left[\left| u(\boldsymbol{\theta}, \overline{t}) \right| \geq u_{\lim} \right] \end{cases} \tag{3}$$

For time-variant reliability problems, an upper bound of the probability of failure, $P_f(T)$, over the time interval $[0, T]$, can be found as

$$P_f(T) \leq \int_0^T \nu_g(t) \mathrm{d}t \tag{4}$$

where $\nu_g(t)$ denotes the mean down-crossing rate of level zero of the limit-state function g. An estimate of $\nu_g(t)$ can be obtained numerically from the limit form relation (Hagen and Tvedt, 1991)

$$\nu_g(t) = \lim_{\delta t \to 0} \frac{P\left[g(\boldsymbol{\theta}, t) > 0 \cap g(\boldsymbol{\theta}, t + \delta t) \leq 0 \right]}{\delta t} \tag{5}$$

The numerical evaluation of the numerator of Equation (5) reduces to a time-invariant two-component parallel system reliability analysis. It is clear that the first part of Equation (3) represents the building block for the solution of both time-invariant and time-variant reliability problems (Der Kiureghian, 1996).

The problem in Equation (1) is extremely challenging for real-world structures and can be solved only in approximate ways. A well established methodology consists of introducing a one-to-one mapping/transformation between the physical space of variables $\boldsymbol{\theta}$ and the standard normal space of variables $\mathbf{y}$ (Ditlevsen and Madsen, 1996) and then computing the probability of failure P_f as

$$P_f = P[G(\mathbf{y}) \le 0] = \int_{G(\mathbf{y})\le 0} \varphi_{\mathbf{Y}}(\mathbf{y})\mathrm{d}\mathbf{y} \tag{6}$$

where $\varphi_{\mathbf{Y}}(\mathbf{y})$ denotes the standard normal joint PDF and $G(\mathbf{y}) = g(\mathbf{r}(\boldsymbol{\theta}(\mathbf{y})), \boldsymbol{\theta}(\mathbf{y}))$ is the limit-state function in the standard normal space.

Solving the integral in Equation (6) remains a formidable task, but this new form of P_f is suitable for approximate solutions taking advantage of the rotational symmetry of the standard normal joint PDF and its exponential decay in both the radial and tangential directions. An optimum point at which to approximate the limit-state surface $G(\mathbf{y}) = 0$ is the 'design point', which is defined as the most likely failure point in the standard normal space, that is, the point on the limit-state surface that is closest to the origin. Finding the design point is a crucial step for approximate methods to evaluate the integral in Equation (6), such as FORM, SORM and importance sampling (Au and Beck, 1999; Breitung, 1984; Der Kiureghian et al., 1987).

The design point, $\mathbf{y}^*$, is found as solution of the following constrained optimisation problem:

$$\mathbf{y}^* = \arg\left\{ \min\left(\frac{1}{2}\mathbf{y}^{\mathrm{T}}\mathbf{y} \right) \middle| G(\mathbf{y}) = 0 \right\} \tag{7}$$

The most effective techniques for solving the constrained optimisation problem in Equation (7) are gradient-based optimisation algorithms (Gill et al., 1981; Liu and Der Kiureghian, 1991) coupled with algorithms for accurate and efficient computation of the gradient of the constraint function $G(\mathbf{y})$, requiring computation of the sensitivities of the response quantities $\mathbf{r}$ to parameters $\boldsymbol{\theta}$. In fact, using the chain rule of differentiation for multivariable functions, we have

$$\nabla_{\mathbf{y}} G = \left(\nabla_{\mathbf{r}} g\big|_{\boldsymbol{\theta}} \cdot \nabla_{\boldsymbol{\theta}}\mathbf{r} + \nabla_{\boldsymbol{\theta}} g\big|_{\mathbf{r}} \right) \nabla_{\mathbf{y}}\boldsymbol{\theta} \tag{8}$$

where $\nabla_{\mathbf{r}} g\big|_{\boldsymbol{\theta}}$ and $\nabla_{\boldsymbol{\theta}} g\big|_{\mathbf{r}}$ are the gradients of limit-state function g with respect to its explicit dependency on quantities $\mathbf{r}$ and $\boldsymbol{\theta}$, respectively, and usually can be computed analytically (e.g. for limit-state function g given in Equation $(2)_1$, we have $\nabla_{\mathbf{r}} g\big|_{\boldsymbol{\theta}} = -1$ and $\nabla_{\boldsymbol{\theta}} g\big|_{\mathbf{r}} = 0$); the term $\nabla_{\boldsymbol{\theta}}\mathbf{r}$ denotes the response sensitivities of response variables $\mathbf{r}$ to parameters $\boldsymbol{\theta}$, and $\nabla_{\mathbf{y}}\boldsymbol{\theta}$ is the gradient of the physical space parameters with respect to the standard normal space parameters (i.e. Jacobian matrix of the probability transformation from the $\mathbf{y}$-space to the $\boldsymbol{\theta}$-space). For probability distribution models defined analytically, the gradient $\nabla_{\mathbf{y}}\boldsymbol{\theta}$ can be derived analytically as well (Ditlevsen and Madsen, 1996).

For real-world problems, the response simulation (computation of $\mathbf{r}$ for given $\boldsymbol{\theta}$) is performed usually using advanced mechanics-based non-linear computational models developed based on the FEM. Finite element reliability analysis requires augmenting existing finite element formulations for response calculation only, to compute the response sensitivities, $\nabla_{\boldsymbol{\theta}}\mathbf{r}$, to parameters $\boldsymbol{\theta}$. An accurate and efficient way to perform finite element response sensitivity analysis is through the DDM (Conte, 2001; Conte et al., 2003; Franchin, 2004; Kleiber et al., 1997; Zhang and Der Kiureghian, 1993; Zona et al., 2005).

3 Material constitutive models

In this paper, two different material constitutive models typically used to describe the behaviour of structural steel are considered: the one-dimensional J_2 plasticity model (also more commonly known as bilinear inelastic model), for which the sensitivity computation algorithm is presented elsewhere (Conte et al., 2003), and the M–P model (1973) in the version extended by Filippou et al. (1983) to account for isotropic strain hardening, for which the response sensitivity computation algorithm is developed and presented in Section 3.2.

The J_2 plasticity model with Von Mises yield surface is a well-known non-smooth plasticity model for metallic materials. Its one-dimensional version presents a kink at the yielding point of the σ-ε relation, leading to discontinuities in response sensitivities at elastic-to-plastic state transition events (Conte, 2001).

The M–P one-dimensional plasticity model is a computationally efficient smooth inelastic model typically used for structural steel, showing very good agreement with experimental results, particularly from cyclic tests on reinforcing steel bars. It presents two favourable features for finite element response, response sensitivity and reliability analyses:

a the model expresses explicitly the current stress as a function of the current strain, so that it is computationally more efficient than competing models such as the Ramberg–Osgood model (Ramberg and Osgood, 1943)

b the constitutive law is smooth and continuously differentiable (with respect to strain and constitutive material parameters), therefore producing response sensitivities continuous everywhere.

Furthermore, the M–P model can accommodate modifications to account for local buckling of steel bars in reinforced concrete members (Monti and Nuti, 1992), and can be used for macroscopic modelling of hysteretic behaviour of structures or substructures with an appropriate choice of the modelling parameters. It is also noteworthy that the M–P model is a physically motivated model of structural material hysteresis, and its performance in representing structural physical behaviour is not undermined by mathematical features that can lead to non-physical analysis results. Such non-physical results have been documented for widely used models such as the Bouc-Wen hysteretic model based on non-linear differential equations (Thyagarajan and Iwan, 1990). Caution is needed in the use of such mathematically-based models to avoid non-physical analysis results, and preference should be granted to physically-based models such as the M–P model used in this paper.

3.1 Response computation

The M–P model is described by the following equations

$$\sigma^* = b\varepsilon^* + \frac{(1-b)\varepsilon^*}{\left(1+\left|\varepsilon^*\right|^R\right)^{1/R}} \tag{9}$$

$$\varepsilon^* = \frac{\varepsilon - \varepsilon_r}{\varepsilon_y - \varepsilon_r} \tag{10}$$

$$\sigma^* = \frac{\sigma - \sigma_r}{\sigma_y - \sigma_r} \tag{11}$$

Equation (9) represents a smooth curved transition from an asymptotic straight line with slope E_0 to another asymptotic straight line with slope E_1, where $b = E_1/E_0$; ε^* and σ^* are the normalised strain and stress, respectively; ε_y and σ_y are the coordinates in the strain-stress plane of the intersection point of the two asymptotes; ε_r and σ_r (initially set to zero) are the coordinates in the strain-stress plane of the point where the last strain reversal event took place; ε and σ are the current strain and stress, respectively; and R is a parameter describing the curvature of the transition curve between the two asymptotes. A typical cyclic stress-strain response behaviour is shown in Figure 1.

Figure 1 Cyclic stress-strain response behaviour of structural steel modelled using M–P model

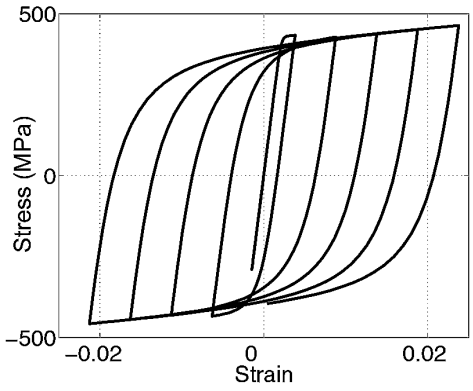

The model is completed by the updating rules for ε_r, σ_r, ε_y, σ_y and R at each strain reversal event. For example, parameter R is obtained as

$$R = R_0 - \frac{a_1\xi}{a_2 + \xi} \tag{12}$$

where R_0 is the value of the parameter R during the first loading; a_1 and a_2 are experimentally determined parameters; ξ is the ratio of the maximum plastic strain $\varepsilon^p_{\max} = \max_{\varepsilon}\left|\varepsilon_{\max} - \varepsilon_y\right|$ over the initial yield strain ε_{y0}. To account for isotropic hardening,

Filippou et al. (1983) proposed a stress shift σ_{sh} in the linear yield asymptote depending on the maximum plastic strain as

$$\frac{\sigma_{sh}}{\sigma_{y0}} = a_3 \left(\frac{\varepsilon_{max}}{\varepsilon_{y0}} - a_4 \right) \tag{13}$$

in which a_3 and a_4 are experimentally determined parameters, ε_{max} is the absolute maximum total strain at the instant of strain reversal and σ_{y0} is the initial yield stress. For this model, the updating rules at the instant of strain reversal (detected in the time step $[t_n,t_{n+1}]$) are

$$\varepsilon_{r,n+1} = \varepsilon_n; \quad \sigma_{r,n+1} = \sigma_n \tag{14}$$

$$\varepsilon^p_{max,n+1} = \begin{cases} \varepsilon^p_{max,n} & \text{if } \varepsilon^p_{max,n} > \left| \varepsilon_n - \varepsilon_{y,n} \right| \\ \left| \varepsilon_n - \varepsilon_{y,n} \right| & \text{otherwise} \end{cases} \tag{15}$$

$$\xi_{n+1} = \frac{\varepsilon^p_{max,n+1}}{\varepsilon_{y0}} \tag{16}$$

$$\varepsilon_{max,n+1} = \begin{cases} \varepsilon_{max,n} & \text{if } \varepsilon_{max,n} > \left| \varepsilon_n \right| \\ \left| \varepsilon_n \right| & \text{otherwise} \end{cases} \tag{17}$$

$$\sigma_{sh,n+1} = \max\left[a_3 \left(\varepsilon_{max,n+1} - a_4 \varepsilon_{y0} \right) E; 0 \right] \tag{18}$$

$$\varepsilon_{y,n+1} = \frac{\sigma_{r,n+1} - E\varepsilon_{r,n+1} \pm \left[(1-b)\sigma_{y0} + \sigma_{sh,n+1} \right]}{(b-1)E} \tag{19}$$

$$\sigma_{y,n+1} = bE\varepsilon_{y,n+1} \pm \left[(1-b)\sigma_{y0} + \sigma_{sh,n+1} \right] \tag{20}$$

In Equations (19) and (20), the '+' sign has to be used for strain inversion from positive strain increment (tensile increment) to negative strain increment (compressive increment), while the '–' sign is required for strain inversion from negative strain increment to positive strain increment.

3.2 Response sensitivity computation

Following the DDM, the exact response sensitivities of the discretised material constitutive laws are required in finite element response sensitivity analysis. The DDM consists of differentiating analytically the space- and time-discretised equations of motion/equilibrium of the finite element model of the structural system considered. It involves

a computing the derivatives (with respect to the sensitivity parameters) of the element and material history/state variables conditional on fixed nodal displacements at the structure level (conditional sensitivities)

b forming the right-hand-side of the response sensitivity equation at the structure level

c solving the resulting equation for the nodal displacement response sensitivities and

d updating the unconditional derivatives of all history/state variables (unconditional sensitivities).

For a more detailed explanation of the DDM, the interested reader is referred elsewhere (Conte, 2001; Conte et al., 1995, 2003, 2004; Barbato and Conte, 2005; Kleiber et al., 1997; Zhang and Der Kiureghian, 1993; Zona et al., 2005). The response sensitivity computation algorithm affects the various hierarchical layers of finite element response calculation, namely the structure, element, section and material levels. This section presents the algorithm for computing the response sensitivities of the M–P material constitutive model over a single time step.

a *Sensitivity parameters* θ: The material constitutive parameters selected as sensitivity parameters are: elastic Young's modulus (E); initial yield stress (σ_{y0}); plastic-to-elastic material stiffness ratio (b).

b *Input at time* $t = t_{n+1}$: The input information for response sensitivity computation at time $t = t_{n+1}$ consists of:

- current strain (ε_{n+1})and stress (σ_{n+1}) and history variables h ($\varepsilon_{r,n+1}$, $\sigma_{r,n+1}$, $\varepsilon^{p}_{\max,n+1}$, ξ_{n+1}, $\varepsilon_{\max,n+1}$ $\sigma_{\mathrm{sh},n+1}$, $\varepsilon_{y,n+1}$, $\sigma_{y,n+1}$) after convergence for the response computation at time t_{n+1}
- unconditional sensitivities at time t_n: $(\mathrm{d}\varepsilon/\mathrm{d}\theta)_n$, $(\mathrm{d}\sigma/\mathrm{d}\theta)_n$, $(\mathrm{d}\varepsilon_r/\mathrm{d}\theta)_n$, $(\mathrm{d}\sigma_r/\mathrm{d}\theta)_n$, $(\mathrm{d}\varepsilon^{p}_{\max}/\mathrm{d}\theta)_n$, $(\mathrm{d}\xi/\mathrm{d}\theta)_n$, $(\mathrm{d}\varepsilon_{\max}/\mathrm{d}\theta)_n$, $(\mathrm{d}\sigma_{\mathrm{sh}}/\mathrm{d}\theta)_n$, $(\mathrm{d}\varepsilon_y/\mathrm{d}\theta)_n$, $(\mathrm{d}\sigma_y/\mathrm{d}\theta)_n$.

c *Algorithm*:

IF strain reversal took place in time step $[t_n, t_{n+1}]$,

THEN compute the sensitivities of all history variables, $(\mathrm{d}h/\mathrm{d}\theta)_{n+1}$, consistently with the constitutive law integration scheme, that is,

$$\left(\frac{\mathrm{d}\varepsilon_r}{\mathrm{d}\theta}\right)_{n+1} = \left(\frac{\mathrm{d}\varepsilon}{\mathrm{d}\theta}\right)_n ; \quad \left(\frac{\mathrm{d}\sigma_r}{\mathrm{d}\theta}\right)_{n+1} = \left(\frac{\mathrm{d}\sigma}{\mathrm{d}\theta}\right)_n \tag{21}$$

$$\left(\frac{\mathrm{d}\varepsilon^{p}_{\max}}{\mathrm{d}\theta}\right)_{n+1} = \begin{cases} \left(\dfrac{\mathrm{d}\varepsilon^{p}_{\max}}{\mathrm{d}\theta}\right)_n & \text{if } \varepsilon^{p}_{\max,n} > \left|\varepsilon_n - \varepsilon_{y,n}\right| \\ \operatorname{sign}(\varepsilon_n - \varepsilon_{y,n})\left[\left(\dfrac{\mathrm{d}\varepsilon}{\mathrm{d}\theta}\right)_n - \left(\dfrac{\mathrm{d}\varepsilon_y}{\mathrm{d}\theta}\right)_n\right] & \text{otherwise} \end{cases} \tag{22}$$

$$\left(\frac{\mathrm{d}\xi}{\mathrm{d}\theta}\right)_{n+1} = \frac{\left(\mathrm{d}\varepsilon^{p}_{\max}/\mathrm{d}\theta\right)_{n+1}\varepsilon_{y0} - \varepsilon^{p}_{\max,n+1}\left(\mathrm{d}\varepsilon_{y0}/\mathrm{d}\theta\right)}{\varepsilon^{2}_{y0}} \tag{23}$$

$$\left(\frac{\mathrm{d}\varepsilon_{\max}}{\mathrm{d}\theta}\right)_{n+1} = \begin{cases} \left(\dfrac{\mathrm{d}\varepsilon_{\max}}{\mathrm{d}\theta}\right)_n & \text{if } \varepsilon_{\max,n} > \left|\varepsilon_n\right| \\ \operatorname{sign}(\varepsilon_n)\left(\dfrac{\mathrm{d}\varepsilon}{\mathrm{d}\theta}\right)_n & \text{otherwise} \end{cases} \tag{24}$$

$$\left(\frac{\mathrm{d}\sigma_{\mathrm{sh}}}{\mathrm{d}\theta}\right)_{n+1} = \begin{cases} a_3\left\{\left(\varepsilon_{\max,n+1} - a_4\varepsilon_{y0}\right)\dfrac{\mathrm{d}E}{d\theta} + \left[\left(\dfrac{\mathrm{d}\varepsilon_{\max}}{\mathrm{d}\theta}\right)_{n+1} - a_4\dfrac{\mathrm{d}\varepsilon_{y0}}{\mathrm{d}\theta}\right]E\right\} & \text{if } \sigma_{\mathrm{sh}} > 0 \\ 0; & \text{otherwise} \end{cases} \tag{25}$$

$$\left(\frac{\mathrm{d}\varepsilon_y}{\mathrm{d}\theta}\right)_{n+1} = \frac{\left(\mathrm{d}\sigma_r/\mathrm{d}\theta\right)_{n+1} - \varepsilon_{r,n+1}\left(\mathrm{d}E/\mathrm{d}\theta\right) - E\left(\mathrm{d}\varepsilon_r/\mathrm{d}\theta\right)_{n+1} \pm \left[(1-b)\left(\mathrm{d}\sigma_{y0}/\mathrm{d}\theta\right) - \sigma_{y0}\left(\mathrm{d}b/\mathrm{d}\theta\right) + \left(\mathrm{d}\sigma_{\mathrm{sh}}/\mathrm{d}\theta\right)_{n+1}\right]}{(b-1)E} - \frac{\left\{\sigma_{r,n+1} - E\varepsilon_{r,n+1} \pm \left[(1-b)\sigma_{y0} + \sigma_{\mathrm{sh},n+1}\right]\right\}\left[E\left(\mathrm{d}b/\mathrm{d}\theta\right) - (1-b)\left(\mathrm{d}E/\mathrm{d}\theta\right)\right]}{(1-b)^2E^2} \tag{26}$$

$$\left(\frac{\mathrm{d}\sigma_y}{\mathrm{d}\theta}\right)_{n+1} = \frac{\mathrm{d}b}{\mathrm{d}\theta}E\varepsilon_{y,n+1} + b\frac{\mathrm{d}E}{\mathrm{d}\theta}\varepsilon_{y,n+1} + bE\left(\frac{\mathrm{d}\varepsilon_y}{\mathrm{d}\theta}\right)_{n+1} \pm \left[(1-b)\frac{\mathrm{d}\sigma_{y0}}{\mathrm{d}\theta} - \sigma_{y0}\frac{\mathrm{d}b}{\mathrm{d}\theta} + \left(\frac{\mathrm{d}\sigma_{sh}}{\mathrm{d}\theta}\right)_{n+1}\right] \tag{27}$$

In Equations (26) and (27), the '+'sign has to be used for strain inversion from positive strain increment (tensile increment) to negative strain increment (compressive increment), while the '−' sign is required for strain inversion from negative strain increment to positive strain increment.

ELSE $(\mathrm{d}h/\mathrm{d}\theta)_{n+1} = (\mathrm{d}h/\mathrm{d}\theta)_n$ (as all the above history variables h remain fixed between two consecutive strain reversal events).

END IF

COMPUTE

$$\left(\frac{\mathrm{d}R}{\mathrm{d}\theta}\right)_{n+1} = -\left(\frac{\mathrm{d}\xi}{\mathrm{d}\theta}\right)_{n+1}\frac{a_1a_2}{\left(a_2+\xi_{n+1}\right)^2} \tag{28}$$

$$\left(\frac{\mathrm{d}\varepsilon^*}{\mathrm{d}\theta}\right)_{n+1} = \frac{\left(\mathrm{d}\varepsilon/\mathrm{d}\theta\right)_{n+1} - \left(\mathrm{d}\varepsilon_r/\mathrm{d}\theta\right)_{n+1}}{\varepsilon_{y,n+1} - \varepsilon_{r,n+1}} - \frac{\left[\left(\mathrm{d}\varepsilon_y/\mathrm{d}\theta\right)_{n+1} - \left(\mathrm{d}\varepsilon_r/\mathrm{d}\theta\right)_{n+1}\right]\left(\varepsilon_{n+1} - \varepsilon_{r,n+1}\right)}{\left(\varepsilon_{y,n+1} - \varepsilon_{r,n+1}\right)^2} \tag{29}$$

$$\left(\frac{\mathrm{d}\sigma^*}{\mathrm{d}\theta}\right)_{n+1} = b\left(\mathrm{d}\varepsilon^*/\mathrm{d}\theta\right)_{n+1} + (\mathrm{d}b/\mathrm{d}\theta)\varepsilon^*_{n+1} + \frac{\left(\mathrm{d}R/\mathrm{d}\theta\right)_{n+1}}{R_{n+1}}\left[\frac{\ln\left|\varepsilon^*_{n+1}\right|\left|\varepsilon^*_{n+1}\right|^{R_{n+1}}}{\left(1+\left|\varepsilon^*_{n+1}\right|^{R_{n+1}}\right)} - \frac{\ln\left(1+\left|\varepsilon^*_{n+1}\right|^{R_{n+1}}\right)}{R_{n+1}}\right] + \frac{(1-b)\left[\left(\mathrm{d}\varepsilon^*/\mathrm{d}\theta\right)_{n+1} - \varepsilon^*_{n+1}\right] - (\mathrm{d}b/\mathrm{d}\theta)\varepsilon^*_{n+1}}{\left(1+\left|\varepsilon^*_{n+1}\right|^{R_{n+1}}\right)^{1/R_{n+1}}} + \frac{\mathrm{sign}\left(\varepsilon^*_{n+1}\right)R_{n+1}\left(\mathrm{d}\varepsilon^*/\mathrm{d}\theta\right)_{n+1}}{\left|\varepsilon^*_{n+1}\right|} \tag{30}$$

$$\left(\frac{\mathrm{d}\sigma}{\mathrm{d}\theta}\right)_{n+1} = \left(\frac{\mathrm{d}\sigma^*}{\mathrm{d}\theta}\right)_{n+1}\left(\sigma_{y,n+1} - \sigma_{r,n+1}\right) + \sigma^*_{n+1}\left[\left(\frac{\mathrm{d}\sigma_y}{\mathrm{d}\theta}\right)_{n+1} - \left(\frac{\mathrm{d}\sigma_r}{\mathrm{d}\theta}\right)_{n+1}\right] + \left(\frac{\mathrm{d}\sigma_r}{\mathrm{d}\theta}\right)_{n+1} \tag{31}$$

END

The DDM requires computing at each analysis step, after convergence is achieved for the response calculation, the structure resisting force sensitivities for nodal displacements kept fixed (i.e. conditional sensitivities). At the material level, the required conditional sensitivities (for ε_{n+1} fixed) can be obtained from Equations (28) to (31) after setting $(\mathrm{d}\varepsilon/\mathrm{d}\theta)_{n+1} = 0$.

4 Application example

A three-story one-bay steel shear-frame is considered as application example in this paper (Figure 2). The structure has been chosen simple enough to allow for closed-form computation of the design point (for pushover analysis and in the case of J_2 plasticity), yet realistic and complex enough to illustrate the main features and difficulties encountered in the general class of problems under study. A key objective of this paper is to show clearly the detrimental effects that discontinuities in finite element response sensitivities could have on the search for the design point(s). More complex examples or more complete and advanced reliability analyses would not achieve this objective as simply and as clearly. In fact, problems of dimension higher than two in the parameter space do not allow simple visualisation of the limit-state function and limit-state surface (visualisation is still possible for limit-state surfaces of three parameter problems). Moreover, other not easily recognisable difficulties for the design point search could be superimposed to the detrimental effects of response sensitivity discontinuities (e.g. multiple design points, saddle points).

Figure 2 Shear-frame structure: geometry, floor displacements and quasi-static horizontal loads

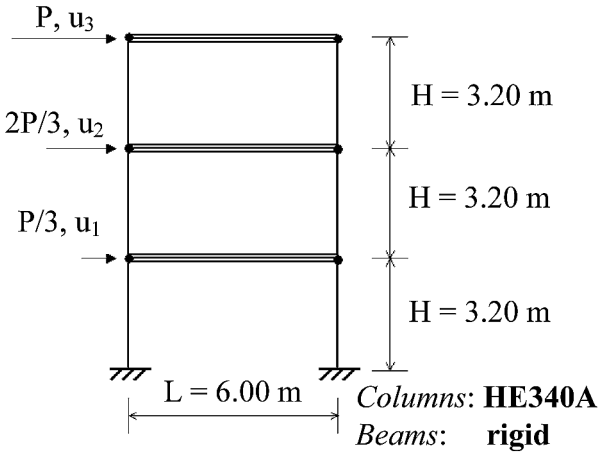

The shear-frame has three stories of height H = 3.20 m each, and one bay of length L = 6.00 m. The columns are European HE340A steel columns with moment of inertia along the strong axis I = 27690.0 cm^4. The steel material has a Young's modulus $E = 2 \times 10^5$ N/mm^2 and an initial yield stress f_{y0} = 350 N/mm^2. The initial yield moment of the columns is M_{y0} = 587.3 kN-m. The beams are considered rigid to enforce a typical shear-building behaviour. Under this assumption, the initial yield shear force for each story is F_{y0} = 734 kN.

The frame described above is assumed to be part of a building structure with a distance between frames L' = 6.00 m. The tributary mass per story, M, is obtained assuming a distributed gravity load of q = 8 kN/m^2, accounting for the structure own weight, as well as for permanent and live loads, and is equal to $M = 28.8 \times 10^3$ kg. The fundamental period of the linear elastic undamped shear-frame is $T_1 = 0.38$ sec. Natural frequencies, natural periods and effective modal mass ratios for the undamped structure are given in Table 1. Viscous damping in the form of Rayleigh damping is assumed with a damping ratio $\xi = 0.05$ for the first and third modes of vibration.

Table 1 Modal analysis results for the linear elastic undamped three-story one-bay shear-frame

Mode #	*Natural circular frequency ω(rad/s)*	*Natural period T (s)*	*Effective modal mass ratio (%)*
1	16.70	0.38	91.41
2	46.80	0.13	7.49
3	67.62	0.09	1.10

The story shear force – interstory drift relation is modelled using three different hysteretic models, which have in common the initial stiffness K = 40.56 kN/mm, the initial yield force F_{y0} = 734 kN and the post-yield stiffness to initial stiffness ratio $b = 0.10$. The three models are:

a M–P model with parameters $R_0 = 20$, $a_1 = 18.5$, $a_2 = 0.15$, $a_3 = a_4 = 0$, denoted as 'M–P ($R_0 = 20$)' in the sequel

b M–P model with parameters $R_0 = 80$, $a_1 = 18.5$, $a_2 = 0.15$, $a_3 = a_4 = 0$, denoted as 'M–P ($R_0 = 80$)' hereafter

c uniaxial J_2 plasticity model with $H_{kin} = K/9 = 4.057$ kN/mm (kinematic hardening modulus), $H_{iso} = 0$ kN/mm (isotropic hardening modulus), and $\alpha_0 = 0$ kN/mm (initial back-stress), denoted as 'J_2 plasticity' hereafter.

The M–P ($R_0 = 20$) model is characterised by typical values of the parameters used for common structural steel, while the M–P ($R_0 = 80$) model is used only for the purpose of reproducing as closely as possible with a smooth inelastic model the behaviour of the non-smooth J_2 plasticity model.

In the following examples, finite element response and response sensitivity analyses are performed using the general-purpose non-linear finite element structural analysis programme FEDEASLab (Filippou and Constantinides, 2004). FEDEASLab is a Matlab (The Mathworks, 1997) toolbox suitable for linear and non-linear, static and dynamic structural analysis, which also incorporates a general framework for parameterisation of finite element models and for response sensitivity computation using the DDM (Franchin, 2004). Reliability analysis is performed using the Matlab-based software FERUM (Haukaas, 2001). The optimisation problem to find the design point(s) is solved using three different optimisation algorithms:

a the (improved) Hasofer-Lind Rackwitz-Fiessler (HL-RF) algorithm (Der Kiureghian and Liu, 1986; Rackwitz and Fiessler, 1978), available in FERUM

b the function FMINCON of the Matlab Optimisation Toolbox (The Mathworks, 2004) and

c the non-linear programming code SNOPT (Gill et al., 2002, 2005).

While the improved HL-RF algorithm is a gradient-based iterative method specialised for structural reliability problems (Liu and Der Kiureghian, 1991), FMINCON and SNOPT are general-purpose optimisation routines based on Sequential Quadratic Programming (SQP) (Gill et al., 1981). The algorithms used by FMINCON and SNOPT are similar for small-scale dense problems (as the ones examined in this paper), with differences involving mainly efficiency and robustness issues. In this paper, the above three different optimisation methods are used to reach a higher confidence level on the results obtained. Research is currently underway to assess the relative performance characteristics of these optimisation methods when applied to structural reliability problems of increasing complexity and dimensionality.

4.1 Finite element response sensitivity analysis

Response sensitivity analysis can be used to gain insight into the effects and relative importance of the loading and material parameters $\boldsymbol{\theta}$ on the response behaviour of a structural system. The example structure presented above is subjected to a response and response sensitivity analysis for quasi-static cyclic loading and dynamic loading in the form of seismic base excitation. Some response quantities and their sensitivities to various material and loading parameters are presented and carefully examined below.

In the quasi-static analysis, horizontal loads are applied at floor levels with an upper triangular distribution, with a maximum load $P = P_{\max}$ at roof level and a total horizontal load (= total base shear) $P_{\text{tot}} = 2P$ (Figure 2). The loading history is presented in the inset of Figure 3.

Figure 3 Total base shear, P_{tot}, versus roof displacement, u_3, for quasi-static cyclic loading and different constitutive models

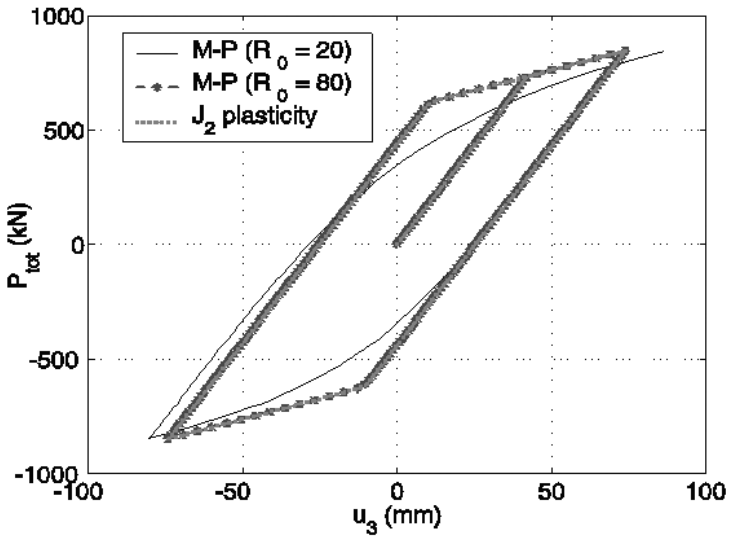

In the main part of Figure 3, the relation between the total base shear P_{tot} and the roof horizontal displacement u_3 is plotted for the three constitutive models considered. After the first unloading (point B), the response of the M–P (R_0 = 20) model deviates significantly from the responses corresponding to the J_2 plasticity and M–P (R_0 = 80) models.

Figures 4 and 5 display the normalised sensitivities of the roof displacement u_3 to the initial yield force F_{y0} and the load parameter P_{max}, respectively. The normalised sensitivities are obtained by multiplying the response sensitivities with the nominal value of the corresponding sensitivity parameters and dividing the results by one hundred. Thus, these normalised sensitivities represent the total change in the response quantity of interest due to 1% change in the sensitivity parameter value and can be used for assessing quantitatively the relative importance of the sensitivity parameters in the deterministic sense. Similar to the response results, the response sensitivities obtained from the J_2 plasticity model are very close to the ones produced by the M–P (R_0 = 80) model and quite different from the ones given by the M–P (R_0 = 20) model. It is important to note that, while the response sensitivities for the J_2 plasticity model are discontinuous at elastic-to-plastic material state transition events, the response sensitivities produced by the M–P models are continuous everywhere (see for example the inset in Figure 4, corresponding to point A in Figure 3). These conclusions are consistent with previous findings of other researchers (Haukaas and Der Kiureghian, 2004).

Figure 4 Normalised sensitivity of roof displacement u_3 to initial yield force F_{y0} (quasi-static cyclic loading)

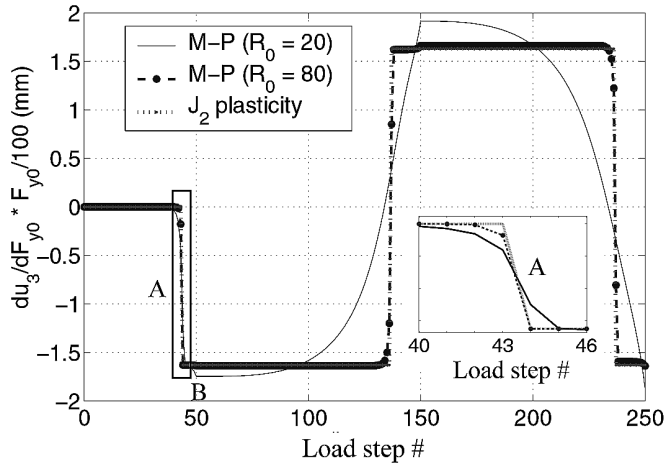

The absence of discontinuities in the response sensitivities for all three constitutive models at unloading events is noteworthy (see for example the inset in Figure 5, corresponding to point B in Figure 3). It has been proven (Haukaas and Der Kiureghian, 2004) that no discontinuities arise from elastic unloading events. This proof assumes explicitly a linear elastic unloading branch in the material constitutive law (as for the uniaxial J_2 plasticity model considered herein) and implicitly that the entire structure (i.e. all yielded integration points) undergoes elastic unloading at the same load/time step. The M–P model presented herein does not have a linear elastic unloading branch; nevertheless, it does not exhibit discontinuities at unloading events as well. It can be proven (see Appendix) that, if only one-dimensional constitutive models are employed,

unloading events in quasi-static finite element analysis do not produce response sensitivity discontinuities provided that the unloading branches of the material constitutive laws can be expanded in Taylor series about the unloading points. A physical explanation of this statement is that any material unloading event can be seen as connecting two stress-strain points on the same (unloading) branch of the constitutive model, as opposed to a material yielding event which connects two stress-strain points belonging to two different branches in the case of a non-smooth constitutive model (see Figure 6).

Figure 5 Normalised sensitivity of roof displacement u_3 to loading parameter P_{max} (quasi-static cyclic loading)

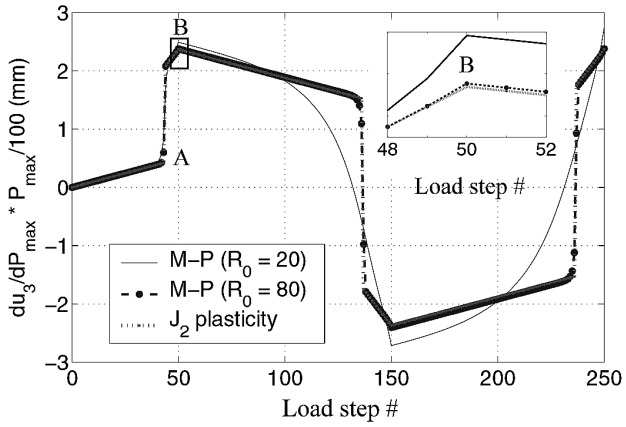

Figure 6 Examples of branches of material constitutive models: (a) loading branch with elastic-to-plastic material state transition (discontinuous response sensitivities) and (b) smooth loading and unloading branches at unloading event (continuous response sensitivities)

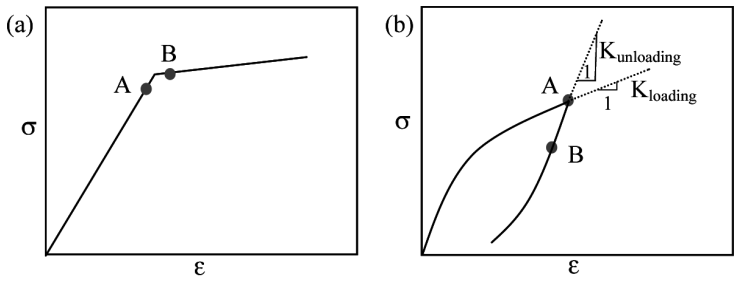

The same example structure is subjected to finite element response and response sensitivity analyses for dynamic seismic loading. The balanced 1940 El Centro earthquake record scaled by a factor 3 is taken as input ground motion with a resulting peak ground acceleration $a_{g,\max} = \max_t\left(\left|\ddot{u}_g(t)\right|\right) = 0.96\ g$. The structure is modelled with the J_2 plasticity, the M–P ($R_0 = 20$) and the M–P ($R_0 = 80$) constitutive law, respectively. Time integration is performed using the constant average acceleration method (special case of the Newmark-beta family of time stepping algorithms that is unconditionally stable, see Appendix for more details). The computed time histories of the roof displacement u_3 are plotted in Figure 7. The results corresponding to the M–P ($R_0 = 80$)

model are not shown, being very close to the ones obtained from the J_2 plasticity model. For all three constitutive models, the structure undergoes large plastic deformations as shown in Figure 7 by the non-zero centred oscillations of the response.

Figure 7 Response histories of roof displacement u_3 for different constitutive models (dynamic analysis)

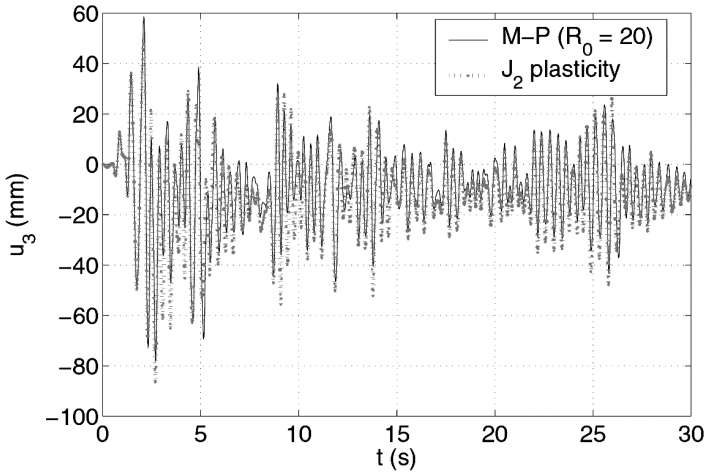

Figures 8 and 9 display the time histories of the normalised sensitivities of the roof displacement u_3 to the initial yield force F_{y0} and the peak ground acceleration $a_{g,\max}$, respectively. Again, the results for the M–P ($R_0 = 80$) model are very similar to those for the J_2 plasticity model and are not shown in Figures 8 and 9. Even a close inspection of these time histories does not reveal any discontinuities in the response sensitivities along the time axis. In fact, both the smoothing effect of the inertia terms in the sensitivity equation of the structure (Haukaas and Der Kiureghian, 2004) and the oscillatory behaviour of the sensitivities contribute to hide discontinuities of small magnitude.

Figure 8 Normalised sensitivity of roof displacement u_3 to initial yield force F_{y0} (dynamic analysis)

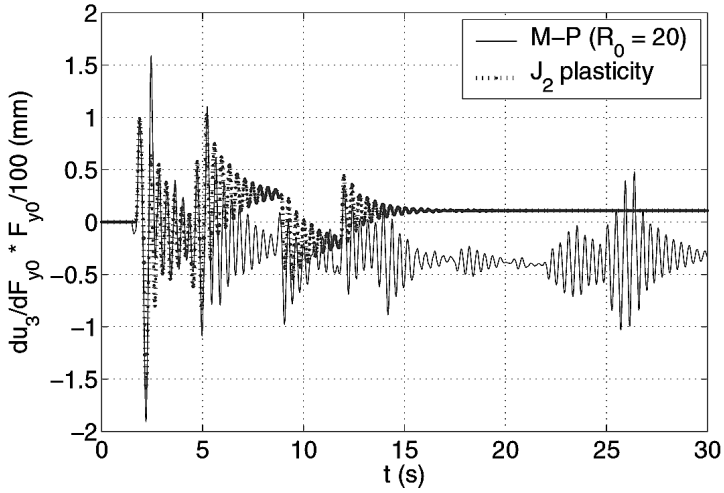

Figure 9 Normalised sensitivity of roof displacement u_3 to peak ground acceleration $a_{g,max}$ (dynamic analysis)

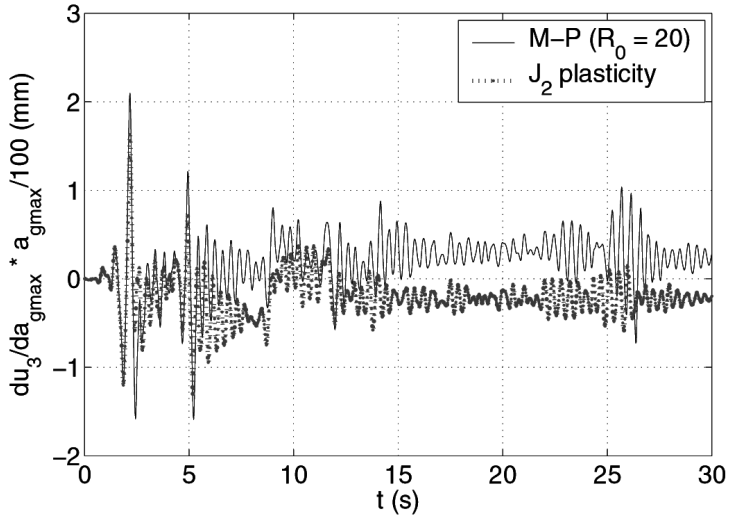

However, examining response sensitivity results along the sensitivity parameter axis (for a fixed time step Δt sufficiently small, herein Δt = 0.001 sec) reveals a very different behaviour: discontinuities arise clearly in the response sensitivities obtained from the non-smooth J_2 plasticity model, while the M–P models response sensitivities are smooth along the parameter axis, as shown in Figure 10. Figures 11 and 12 plot the time histories (for $0 \le t \le 5$ sec) of the displacement u_3 for fixed peak ground acceleration $a_{g,max}$ and variable initial yield force F_{y0} obtained using the M–P (R_0 = 20) model and the J_2 plasticity model, respectively, and the integration time step Δt = 0.001 sec. It is observed that the response surfaces are continuous in both time and parameter F_{y0} and present small differences overall between the two different constitutive models. Figures 13 and 14 show the time histories (for $0 \le t \le 5$ sec) of the normalised sensitivities of the displacement u_3 to the initial yield force F_{y0} for fixed peak ground acceleration $a_{g,max}$ and variable initial yield force F_{y0} obtained using the M–P (R_0 = 20) model and the J_2 plasticity model, respectively, and the integration time step Δt = 0.001 sec. The response sensitivity surface obtained for the M–P (R_0 = 20) constitutive model is continuous in both time and parameter F_{y0}, whereas the response sensitivity surface obtained using the J_2 plasticity model exhibits clear discontinuities along the parameter axis. It is important to notice that continuity along the parameter axis is obtained only for a sufficiently small integration time step Δt (see Appendix). If the time step used to integrate the equations of motion of the system is not small enough, spurious discontinuities can be introduced by the time stepping scheme employed, as illustrated in Figure 15, which shows the surface of the normalised sensitivities of the displacement u_3 to the initial yield force F_{y0} for fixed peak ground acceleration $a_{g,max}$ and variable initial yield force F_{y0} obtained using the M–P (R_0 = 20) model and the integration time step Δt = 0.02 sec.

Figure 10 Normalised sensitivity of roof displacement u_3 to initial yield force F_{y0} at time $t = 1.66$ sec with fixed peak ground acceleration $a_{g,max}$

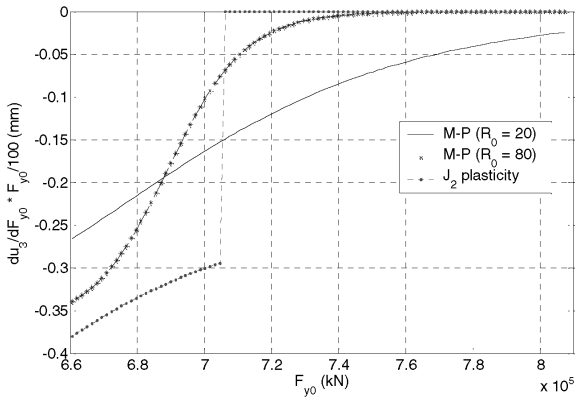

Figure 11 Time histories (for $0 \le t \le 5$sec) of displacement u_3 for fixed peak ground acceleration $a_{g,max}$ and variable initial yield force F_{y0}: dynamic analysis using the M–P ($R_0 = 20$) model and $\Delta t = 0.001$ sec

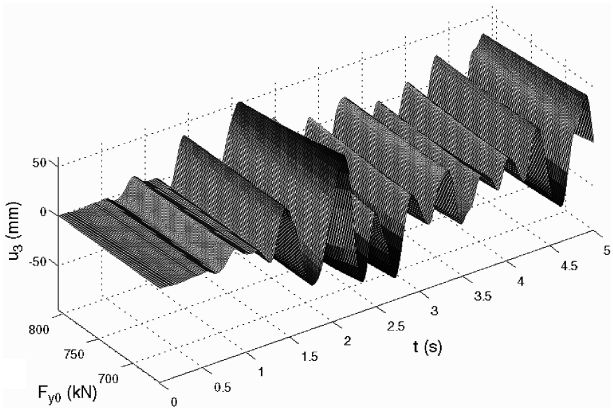

Figure 12 Time histories (for $0 \le t \le 5$ sec) of displacement u_3 for fixed peak ground acceleration $a_{g,max}$ and variable initial yield force F_{y0}: dynamic analysis using the J_2 plasticity model and $\Delta t = 0.001$ sec

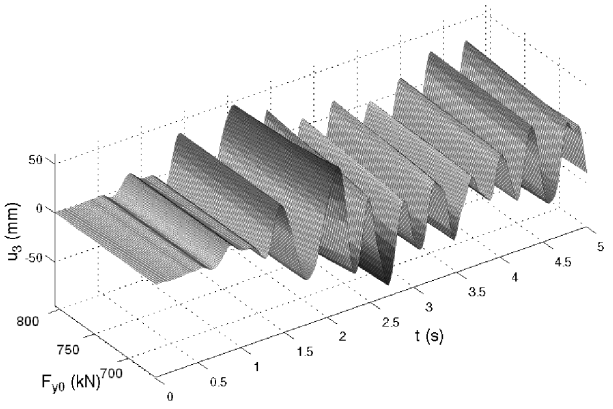

Figure 13 Time histories (for $0 \le t \le 5$ sec) of normalised sensitivities of the displacement u_3 to initial yield force F_{y0} for fixed peak ground acceleration $a_{g,max}$ and variable initial yield force F_{y0}: dynamic analysis using the M–P ($R_0 = 20$) model and $\Delta t = 0.001$ sec

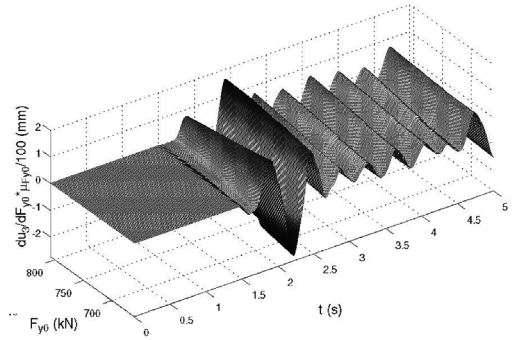

Figure 14 Time histories (for $0 \le t \le 5$ sec) of normalised sensitivities of the displacement u_3 to initial yield force F_{y0} for fixed peak ground acceleration $a_{g,max}$ and variable initial yield force F_{y0}: dynamic analysis using the J_2 plasticity model and $\Delta t = 0.001$ sec

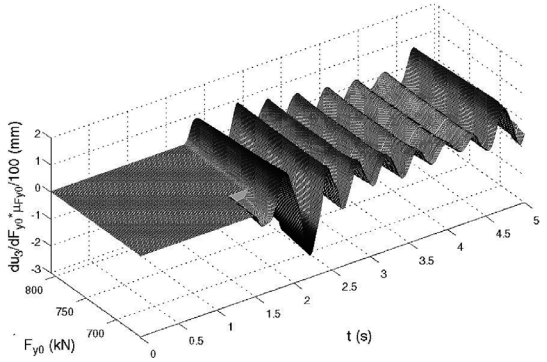

Figure 15 Time histories (for $0 \le t \le 5$ sec) of normalised sensitivities of the displacement u_3 to initial yield force F_{y0} for fixed peak ground acceleration $a_{g,max}$ and variable initial yield force F_{y0}: dynamic analysis using the M–P ($R_0 = 20$) model and $\Delta t = 0.02$ sec

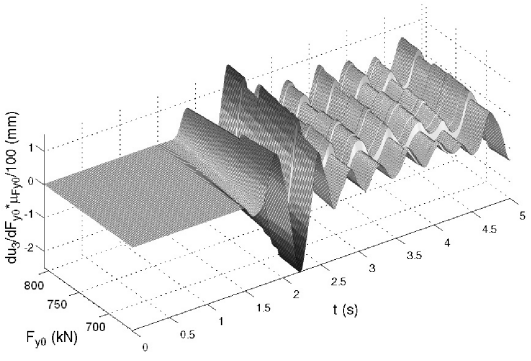

In finite element reliability analysis, response sensitivity discontinuities in the parameter space can be detrimental to the convergence of the computational optimisation procedure to find the design point(s). Therefore, the use of smooth constitutive laws is also

beneficial in the dynamic case for avoiding discontinuities in the response sensitivities along the parameter axes, provided that the integration time step is small enough.

4.2 Time-invariant reliability analysis: probabilistic pushover analysis

In this section, the same example structure is subjected to a probabilistic pushover analysis based on the same upper triangular distribution of horizontal loads defined in the previous section (Figure 2). The load variable P increases monotonically from zero to $P_{\max}$. The load parameter $P_{\max}$ and the initial yield shear force F_{y0} are modelled as random variables and a limit-state function g is defined in terms of the maximum roof displacement u_3 up-crossing the threshold level $u_{\lim}$ as

$$g = u_{\lim} - u_3\left(F_{y0}, P_{\max}\right) \tag{32}$$

For the given shear-frame structure with the story shear behaviour modelled using the J_2 plasticity model, the above limit-state function can be obtained in closed-form from structural analysis principles. The limit-state function consists of the union of four planar surfaces (in the $P_{\max}$–F_{y0} –g space), each surface corresponding to a different number of yielded stories of the shear frame. For the same structure modelled using the M–P constitutive model, a closed-form expression of the limit-state function is not available and the function g can only be evaluated numerically.

The two uncertain/random parameters $P_{\max}$ and F_{y0} are assumed to be independent Gaussian random variables with mean and standard deviation $\mu_{P_{\max}}$ = 424 kN, $\sigma_{P_{\max}}$ = 42.4 kN for $P_{\max}$ and $\mu_{F_{y0}}$ = 734 kN, $\sigma_{F_{y0}}$ = 36.7 kN for F_{y0}, respectively. The choice of Gaussian distributions allows to conveniently keep the piecewise linear geometry of the limit-state function in the transformation from the physical parameter space (F_{y0}, $P_{\max}$,) to the standard normal space ($U_{F_{y0}}$, $U_{P_{\max}}$).

The limit-state function in the standard normal space for the J_2 plasticity model can again be obtained in closed-form as a linear transformation of the limit-state function in the physical space. For any specified value of $u_{\lim}$, the limit-state surface is piecewise linear as the response function u_3 is a surface obtained as the union of planar surfaces joined by straight lines corresponding to the yield points of the shear-frame stories (Figure 16(a)). Figure 16(b) shows the response surface for quasi-static pushover of the example structure modelled using the M–P (R_0 = 20) smooth constitutive model.

For the example structure modelled using the J_2 plasticity constitutive law, the design point in the standard normal space, $\boldsymbol{U}^* = (U^*_{F_{y0}}, U^*_{P_{\max}})$, can also be found in closed-form as function of the threshold level $u_{\lim}$ as

$$\boldsymbol{U}^* \equiv \begin{cases} U^*_{\mathrm{F}_{y0}} = 0, & U^*_{\mathrm{P}_{\max}} = .205u_{\lim} - 10; & u_{\lim} < 42.22 \\ U^*_{\mathrm{F}_{y0}} = .474u_{\lim} - 20, & U^*_{\mathrm{P}_{\max}} = .205u_{\lim} - 10; & 42.22 \le u_{\lim} < 43.07 \\ U^*_{\mathrm{F}_{y0}} = -.013u_{\lim} + .961, & U^*_{\mathrm{P}_{\max}} = .038u_{\lim} - 2.796; & 43.07 \le u_{\lim} < 82.73 \\ U^*_{\mathrm{F}_{y0}} = -.009u_{\lim} + .610, & U^*_{\mathrm{P}_{\max}} = .022u_{\lim} - 1.475; & 82.73 \le u_{\lim} < 408.70 \\ U^*_{\mathrm{F}_{y0}} = -.008u_{\lim} - .006, & U^*_{\mathrm{P}_{\max}} = .016u_{\lim} + .013; & u_{\lim} \ge 408.70 \end{cases} \tag{33}$$

in which u_{lim} is expressed in mm. Figure 17 shows the locus of the design point for variable u_{lim}, when the structure is modelled using the J_2 plasticity model, in the domain $\left[-2 \le U_{F_{y0}} \le 2; -2 \le U_{P_{\max}} \le 2\right]$ (thick black line). On the same figure, the projections of the lines on the limit-state function corresponding to yielding of the first and second stories are plotted together with some representative limit-state surfaces corresponding to specified values of u_{lim}, namely,

a $u_{\text{lim}} = 41.46$ mm (design point on the first branch of the locus of the design point)

b $u_{\text{lim}} = 42.50$ mm (design point on the second branch of the locus of the design point)

c $u_{\text{lim}} = 80.14$ mm (design point on the third branch of the locus of the design point) and

d $u_{\text{lim}} = 100.00$ mm (design point on the fourth branch of the locus of the design point).

Figure 16 Response surfaces for quasi-static pushover analysis of example structure modelled using: (a) J_2 plasticity model and (b) M–P ($R_0 = 20$) model

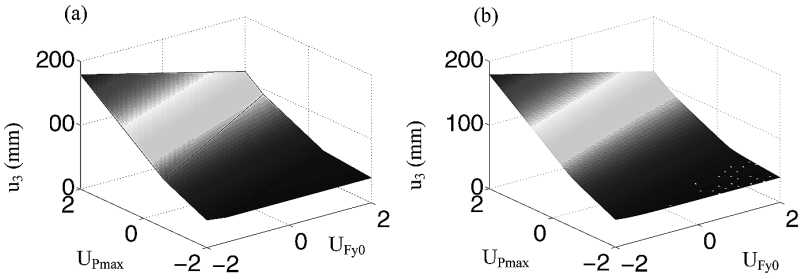

Figure 17 Locus of the design points for varying u_{lim}, when the example structure is modelled using the J_2 plasticity model (probabilistic pushover analysis)

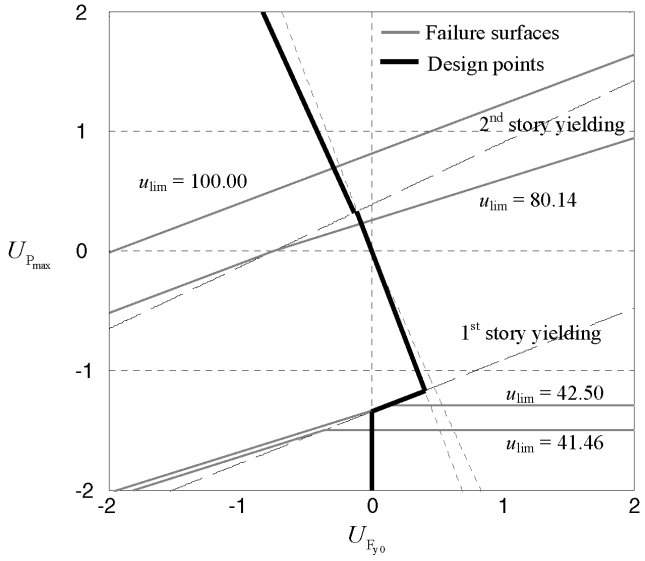

Furthermore, it can be readily shown that, if the structure is modelled using the J_2 plasticity model, in the range 42.22 mm $\leq u_{\text{lim}} \leq$ 43.07 mm (second branch of the locus of the design point), the design point is located at a kink of the limit-state surface, and is not an origin projected point. In this case, the design point cannot be found with a gradient-based optimisation algorithm. For values of the threshold level outside this range, the design point is located on one of the linear branches of the limit-state surface and its search is not hampered by non-smoothness of the material constitutive model.

The same probabilistic pushover analysis is performed on the example structure modelled using the M–P constitutive model (with R_0 = 20 and R_0 = 80) with u_{lim} = 42.5 mm (value for which a gradient-based optimisation algorithm fails to converge to the design point in the case of the J_2 plasticity model). This unrealistically low threshold is chosen for illustrating aspects of convergence to the design point(s) that could also apply to more realistic cases. In this case, using the improved Hasofer-Lind Rackwitz-Fiessler (HL-RF) algorithm (Liu and Der Kiureghian, 1991) for the design point search, the design point is found in seven iterations and the corresponding reliability index is $\beta = -1.29$. The same results are obtained using FMINCON and SNOPT, with a similar number of function evaluations.

A comparison between Figure 16(a) and (b) indicates that the response surfaces for the J_2 plasticity and M–P (R_0 = 20) constitutive model, respectively, are numerically very close, but only the one corresponding to the M–P model is smooth and continuously differentiable everywhere. In Figure 18, the sensitivities of the roof displacement u_3 to the initial yield force F_{y0} (normalised with the mean value of the sensitivity parameter μ_{Fy0}) are shown for both:

a the J_2 plasticity and

b the M–P (R_0 = 20) models.

Figure 18 Normalised sensitivities of roof displacement u_3 to initial yield force F_{y0} for varying F_{y0}: (a) J_2 plasticity model and (b) M–P (R_0 = 20) model

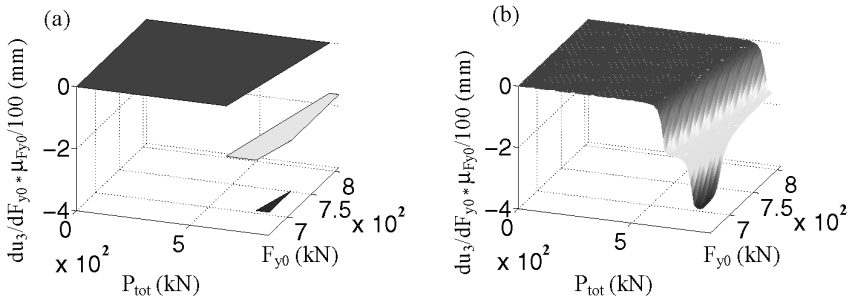

Again, the response sensitivities for the J_2 plasticity model are discontinuous, whereas the M–P model produces continuous (and smooth) sensitivities.

The numerical results of the three probabilistic pushover analyses (for the three constitutive models) are summarised in Table 2 and the corresponding limit-state surfaces and design points are shown in Figure 19. The limit-state surface for the J_2 plasticity model is piecewise linear and made of four branches. The probability of failure for the structure modelled with the J_2 plasticity constitutive law is evaluated numerically from the exact solution considering the problem as a four component series system

(requiring computation of a four-variate standard normal cumulative distribution function). It is noteworthy that the approximate solution obtained considering only the two of the four components with lower absolute value of the reliability index β_i (i = 1,2,3,4) practically coincides with the exact solution (P_f = 0.9101), whereas the value for the probability of failure obtained using a FORM approximation based only on the distance $|\beta|$ of the design point from the origin ($P_{f,\mathrm{FORM}} = \Phi(-\beta) = 0.9022$, where Φ denotes the uni-variate standard normal cumulative distribution function) is less accurate. Obviously, in the present case, accuracy is not a real concern because of the unrealistically high value of the probability of failure. However, for other applications it may be necessary to have accurate evaluation of the probability content of the safe domain (e.g. when solving a mean-outcrossing rate problem as a two-component parallel system).

Table 2 Reliability analysis results for quasi-static pushover with u_{lim} = 42.5 mm

	J_2 plasticity model Exact solution	*M–P (R_0 = 20) model FORM*	*M–P (R_0 = 80) model FORM*
β	−1.2943	−1.4415	−1.3224
P_f	0.9101	0.9253	0.9070
P_{max}* (kN)	369.41	362.88	367.93
F_{y0}* (kN)	738.81	741.51	740.42
# of iterations	–	7	11

Figure 19 Limit-state surfaces (l-s. s.) and design points (d. p.) for u_{lim} = 42.5mm (probabilistic pushover analysis)

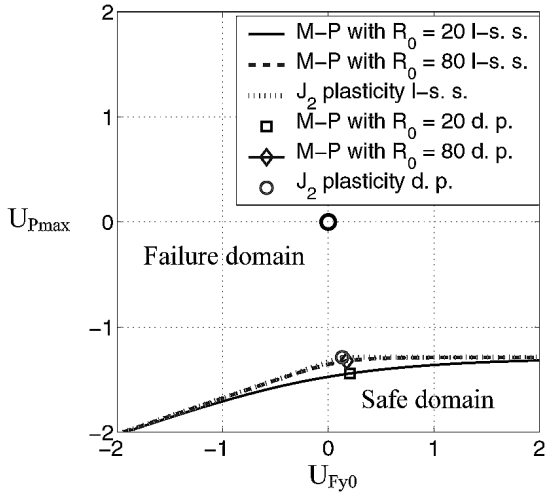

It is important to report that the improved HL-RF algorithm is not able to converge to the design point in the case of the example structure modelled with the J_2 plasticity constitutive law; after about ten iterations, it enters an infinite iteration cycle (i.e. cycling over the same set of three points). Failure to converge to the design point in this particular case is due to the response sensitivity discontinuity exactly located at the

design point (see Figure 19). The same convergence difficulties are encountered using FMINCON and SNOPT and are typical of any gradient-based optimisation technique when discontinuities are located near the searched local optimum.

4.3 Time-variant reliability analysis: mean out-crossing rate computation

An analysis for computing the mean down-crossing rate of the roof displacement u_3 below the threshold $u_{\text{lim}} = -33$ mm at time $t = 1.66$ sec was performed on the same example structure. Both the threshold value and the time were selected for convenience purposes. The input ground motion was taken as the balanced 1940 El Centro earthquake record scaled by a factor 3. The peak ground motion acceleration $a_{g,\max}$ and the initial yield force F_{y0} are modelled as statistically independent Gaussian random variables with mean and standard deviation $\mu_a = 9.38$ m/s^2, $\sigma_a = 0.938$ m/s^2 for $a_{g,\max}$ and $\mu_{F_{y0}} = 734$ kN, $\sigma_{F_{y0}} = 36.7$ kN for F_{y0}, respectively.

In Figure 20, the response surfaces of the roof displacement u_3 at time $t = 1.66$ sec, obtained from deterministic dynamic analyses varying parameters $a_{g,\max}$ and F_{y0} (over a fine grid) are plotted for the structure modelled with the:

a J_2 plasticity model and

b M–P ($R_0 = 20$) constitutive model, respectively.

Figure 20 Response surfaces at time $t = 1.66$ sec for dynamic analysis of example structure modelled with: (a) J_2 plasticity model and (b) M–P ($R_0 = 20$) model

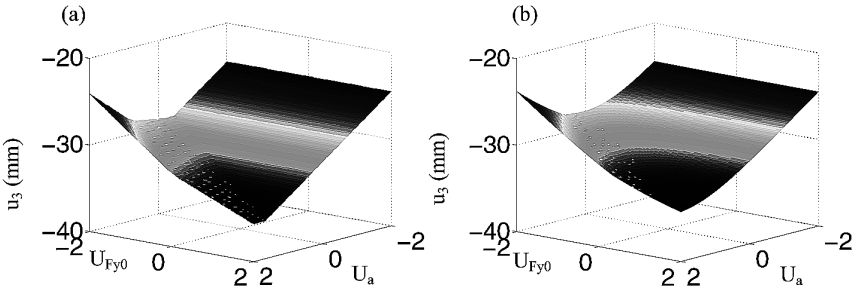

Figure 21 shows the limit-state surfaces and the design points for the three constitutive models considered and for the threshold $u_{\text{lim}} = -33$ mm. For each constitutive model, computation of the mean out-crossing rate at a prescribed time t requires two design point searches corresponding to the limit-state surfaces at times t and $t + \delta t$, respectively (here $\delta t = 10^{-4}$ sec).

For this dynamic example, no closed-form expression is available for the response of the structure with the J_2 plasticity model. Therefore, no closed-form solutions are available for the limit-state surface and its kinks, the design point (shown in Figure 21) and mean out-crossing rate. As for the quasi-static case in Section 4.2, the modified HL-RF (gradient-based) algorithm is not able to provide a converged numerical estimate of the design points. However, no difficulties are encountered in the design point search for the M–P constitutive models, for which the FORM approximation of the mean down-crossing rate ν_{u_3} of the roof displacement u_3 below the threshold $u_{\text{lim}} = -33$ mm at time $t = 1.66$ sec is 21.07 s^{-1} ($R_0 = 20$) and 57.72 s^{-1} ($R_0 = 80$), respectively. The high

values obtained for the instantaneous mean down-crossing rates are due to the deterministic shape of the input ground motion. In fact, crossings of a deterministic threshold are more likely to occur in correspondence with peaks and valleys in the time history of the response quantity considered, while they have a very low probability of occurrence elsewhere. Thus, the time history of the mean up/down/out-crossing rate consists of a sequence of very narrow peaks, usually well spaced along the time axis.

Figure 21 Limit-state surfaces (l-s. s.) and design points (d. p.) for $u_{lim} = -33$ mm at time $t = 1.66$ sec (dynamic analysis)

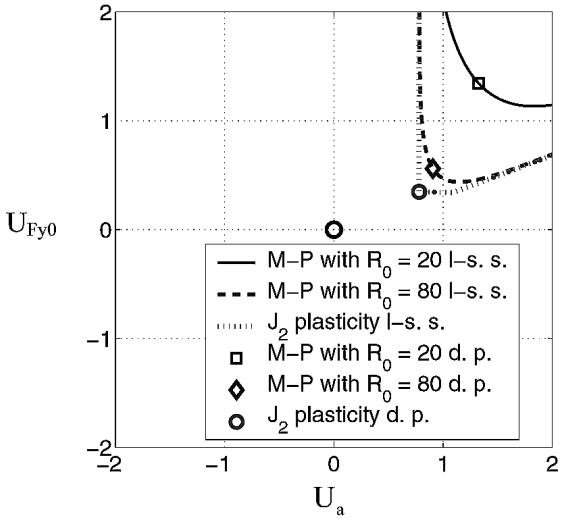

In general, for both quasi-static and dynamic analysis, gradient-based optimisation algorithms do not ensure convergence to a (local) optimum of the objective function subject to the given constraints (expressed in terms of structural response quantities) if response sensitivities are discontinuous. Typically, non-convergence to an existing optimum happens if discontinuities in the gradient of the limit-state function (i.e. response sensitivity discontinuities) occur in a neighborhood of the optimum itself. Even in cases when convergence can be achieved, gradient discontinuities could be detrimental to the convergence rate of the optimisation procedure. In theory, gradient-based optimisation algorithms can reach (locally) a quadratic convergence rate, when the Lagrangian function associated with the given problem is second-order differentiable and its exact Hessian is available (Gill et al., 1981). However, this is not the case for structural reliability problems, for which at most first-order response sensitivities are available. It can thus be concluded that, for general/practical purposes in finite element reliability analysis, requiring at least continuous finite element response sensitivities is a good compromise between convergence rate and computational cost.

5 Conclusions

Insight is gained into the analytical behaviour of finite element response sensitivities obtained from smooth (M–P) and non-smooth (J_2 plasticity) material constitutive models. The response sensitivity computation algorithm for the M–P uniaxial

material constitutive model is developed and presented. Focus is on continuity (or discontinuity) of finite element response sensitivities. In particular, important response sensitivity discontinuities are observed along the axes of both pseudo-time and sensitivity parameters when using non-smooth material models in quasi-static finite element analysis. A sufficient condition is stated and proved on the smoothness properties of material constitutive laws for obtaining continuous response sensitivities in the quasi-static analysis case. These results about response sensitivity continuity are illustrated using the M–P material constitutive law to model a simple inelastic steel shear-frame. Comparisons are made between response and response sensitivities obtained using the smooth M–P and the non-smooth uniaxial J_2 plasticity material constitutive law to model the same example structure. Response and response sensitivity computations are also examined in the dynamic analysis case using both the M–P and J_2 plasticity models. It is found that the linear inertia and damping terms in the equations of motion have significant smoothing effects on the response sensitivity results along the time axis. Nevertheless, discontinuities along the parameter axes are observed for both non-smooth and smooth constitutive models, if the time discretisation of the equations of motion is not sufficiently refined. Important remarks and observations are made about the dynamic analysis case, which suggest that response sensitivity discontinuities can be eliminated by using smooth material constitutive models and refining the time discretisation of the equations of motion. Some of the discontinuities in dynamic response sensitivities obtained using non-smooth material constitutive models are inherent to the constitutive models themselves and cannot be eliminated by reducing the integration time step. Response sensitivity results are presented in support of these conclusions.

The importance of the continuity of response sensitivities for the design point search using gradient-based optimisation algorithms is highlighted with an example of probabilistic pushover analysis and an example of mean out-crossing rate computation performed on a simple inelastic steel shear-frame. It is observed that, when discontinuities are present in the response sensitivities, convergence to a (local) design point cannot be ensured by gradient-based optimisation techniques.

The limit-state function visualisation provided for the relatively simple example with a two-dimensional random parameter space considered in this paper needs to be generalised to higher dimensional parameter spaces in which ‘kink-points’ (observed in the example herein) generalise to ‘kink-hypersurfaces’. More insight about the topology of the failure domains for both quasi-static and dynamic problems (with uncertain/random loading and system parameters) may lead to new, more robust and more efficient algorithmic approaches for finite element reliability analysis.

Acknowledgements

Partial supports of this research by the National Science Foundation under Grant No. CMS-0010112 and by the Pacific Earthquake Engineering Research (PEER) Center through the Earthquake Engineering Research Centers Program of the National Science Foundation under Award No. EEC-9701568 are gratefully acknowledged. Any opinions, findings, conclusions or recommendations expressed in this publication are those of the authors and do not necessarily reflect the views of the sponsors.

References

Ang, G.L., Ang, A.H-S. and Tang, W.H. (1992) 'Optimal importance sampling density estimator', *Journal of Engineering Mechanics (ASCE)*, Vol. 118, No. 6, pp.1146–1163.

Au, S.K. and Beck, J.L. (1999) 'A new adaptive importance sampling scheme', *Structural Safety*, Vol. 21, No. 2, pp.135–158.

Au, S.K. and Beck, J.L. (2001a) 'First excursion probabilities for linear systems by very efficient importance sampling', *Probabilistic Engineering Mechanics*, Vol. 16, No. 3, pp.193–207.

Au, S.K. and Beck, J.L. (2001b) 'Estimation of small failure probabilities in high dimensions by subset simulation', *Probabilistic Engineering Mechanics*, Vol. 16, No. 4, pp.263–277.

Au, S.K. and Beck, J.L. (2003) 'Subset simulation and its application to seismic risk based on dynamic analysis', *Journal of Engineering Mechanics (ASCE)*, Vol. 129, No. 8, pp.901–917.

Au, S.K., Papadimitriou, C. and Beck, J.L. (1999) 'Reliability of uncertain dynamical systems with multiple design points', *Structural Safety*, Vol. 21, No. 2, pp.113–133.

Barbato, M. and Conte, J.P. (2005) 'Finite element response sensitivity analysis: a comparison between force-based and displacement-based frame element models', *Computer Methods in Applied Mechanics and Engineering*, Vol. 194, Nos. 12–16, pp.1479–1512.

Breitung, K. (1984) 'Asymptotic approximations for multinormal integrals', *Journal of the Engineering Mechanics Division, ASCE*, Vol. 110, No. 3, pp.357–366.

Bucher, C.G. (1988) 'Adaptive importance sampling – an iterative fast Monte Carlo procedure', *Structural Safety*, Vol. 5, No. 2, pp.119–126.

Conte, J.P., Jagannath, M.K. and Meghella, M. (1995) 'Earthquake response sensitivity analysis of concrete gravity dams', *Proceedings of Seventh International Conference on Applications of Statistics and Probability*, Paris, France, 10–13 July, pp.395–402.

Conte, J.P. (2001) 'Finite element response sensitivity analysis in earthquake engineering', *Earthquake Engineering Frontiers in the New Millennium*, Spenser and Hu, Swets and Zeitlinger, pp.395–401.

Conte, J.P., Barbato, M. and Spacone, E. (2004) 'Finite element response sensitivity analysis using force-based frame models', *International Journal for Numerical Methods in Engineering*, Vol. 59, No. 13, pp.1781–1820.

Conte, J.P., Vijalapura, P.K. and Meghella, M. (2003) 'Consistent finite-element response sensitivity analysis', *Journal of Engineering Mechanics (ASCE)*, Vol. 129, No. 12, pp.1380–1393.

Der Kiureghian, A. and Liu, P-L. (1986) 'Structural reliability under incomplete probability information', *Journal of the Engineering Mechanics Division (ASCE)*, Vol. 111(EM1), pp.85–104.

Der Kiureghian, A., Lin, H-Z. and Hwang, S-J. (1987) 'Second-order reliability approximations', *Journal of the Engineering Mechanics Division (ASCE)*, Vol. 113(EM8), pp.1208–1225.

Der Kiureghian, A. and Ke, B-J. (1988) 'The stochastic finite element method in structural reliability', *Probabilistic Engineering Mechanics*, Vol. 3, No. 2, pp.83–91.

Der Kiureghian, A. (1996) 'Structural reliability methods in seismic safety assessment: a review', *Journal of Engineering Structures*, Vol. 18, No. 6, pp.412–424.

Ditlevsen, O. and Madsen, H.O. (1996) *Structural Reliability Methods*, New York: Wiley.

Filippou, F.C. and Constantinides, M. (2004) 'FEDEASLab getting started guide and simulation examples', *Technical Report NEESgrid-2004-22*, 31 August, Available at: http://fedeaslab.berkeley.edu/.

Filippou, F.C., Popov, E.P. and Bertero, V.V. (1983) 'Effects of bond deterioration on hysteretic behavior of reinforced concrete joints', *Report EERC 83–19*, Earthquake Engineering Research Center, University of California, Berkeley.

Franchin, P. (2004) 'Reliability of uncertain inelastic structures under earthquake excitation', *Journal of Engineering Mechanics (ASCE)*, Vol. 130, No. 2, pp.180–191.

Gill, P.E., Murray, W. and Wright, M.H. (1981) *Practical Optimization*, New York: Academic Press.

Gill, P.E., Murray, W. and Saunders, M.A. (2002) 'SNOPT: an SQP algorithm for large-scale constrained optimization', *SIAM Journal on Optimization*, Vol. 12, pp.979–1006.

Gill, P.E., Murray, W. and Saunders, M.A. (2005) 'User's guide for SNOPT version 7, a Fortran package for large-scale non-linear programming', *User's Guide*, Version 7.0, Available at: http://www.scicomp.ucsd.edu/~peg/.

Gu, Q. and Conte, J.P. (2003) 'Convergence studies in non-linear finite element response sensitivity analysis', *Applications of Statistics and Probability in Civil Engineering*, *Proceedings of ICASP9*, San Francisco, CA, 6–9 July, Rotterdam, Netherlands: Millpress.

Hagen, O. and Tvedt, L. (1991) 'Vector process out-crossing as parallel system sensitivity measure', *Journal of Engineering Mechanics (ASCE)*, Vol. 117, No. 10, pp.2201–2220.

Haukaas, T. (2001) 'FERUM (Finite Element Reliability Using Matlab)', *User's Guide*, Version 3.0, Available at: http://www.ce.berkeley.edu/~haukaas/FERUM/ferum.html.

Haukaas, T. and Der Kiureghian, A. (2004) 'Finite element reliability and sensitivity methods for performance-based engineering', *Report PEER 2003/14*, Pacific Earthquake Engineering Research Center, University of California, Berkeley.

Hohenbichler, M. and Rackwitz, R. (1986) 'Sensitivity and importance measures in structural reliability', *Civil Engineering Systems*, Vol. 3, No. 4, pp.203–209.

Hughes, T.J.R. (1987) *The Finite Element Method – Linear Static and Dynamic Finite Element Analysis*, Englewood Cliffs, NJ: Prentice-Hall.

Kleiber, M., Antunez, H., Hien, T.D. and Kowalczyk, P. (1997) *Parameter Sensitivity in Non-linear Mechanics: Theory and Finite Element Computation*, New York, Wiley.

Liu, P-L. and Der Kiureghian, A. (1991) 'Optimization algorithms for structural reliability', *Structural Safety*, Vol. 9, No. 3, pp.161–177.

Melchers, R.E. (1989) 'Importance sampling in structural systems', *Structural Safety*, Vol. 6, No. 1, pp.3–10.

Menegotto, M. and Pinto, P.E. (1973) 'Method for analysis of cyclically loaded reinforced concrete plane frames including changes in geometry and non-elastic behavior of elements under combined normal force and bending', *Proceedings*, *IABSE Symposium on 'Resistance and Ultimate Deformability of Structures Acted on by Well-Defined Repeated Loads'*, Lisbon.

Monti, G. and Nuti, C. (1992) 'Non-linear cyclic behavior of reinforcing bars including buckling', *Journal of Structural Engineering (ASCE)*, Vol. 118, No. 12, pp.3268–3284.

Rackwitz, R. and Fiessler, B. (1978) 'Structural reliability under combined random load sequences', *Computers and Structures*, Vol. 9, No. 5, pp.489–499.

Ramberg, W. and Osgood, W.R. (1943) 'Description of stress-strain curves by three parameters', *Technical Note 902*, NACA.

Schueller, G.I., Pradlwarter, H.J. and Koutsourelakis, P.S. (2004) 'A critical appraisal of reliability estimation procedures for high dimensions', *Probabilistic Engineering Mechanics*, Vol. 19, No. 4, pp.463–474.

Schueller, G.I. and Stix, R. (1987) 'A critical appraisal of methods to determine failure probabilities', *Structural Safety*, Vol. 4, No. 4, pp.293–309.

Simo, J.C. and Hughes, T.J.R. (1998) *Computational Inelasticity*, Springer Verlag.

Thyagarajan, R.S. and Iwan, W.D. (1990) 'Performance characteristics of a widely used hysteretic model in structural dynamics', *Proceedings of the Fourth US National Conference on Earthquake Engineering*, *EERI*, Palm Springs, Vol. 2, pp. 177–186.

The MathWorks (1997) 'Matlab – high performance numeric computation and visualization software', *User's Guide*, Natick, MA: The MathWorks, Inc.

The MathWorks (2004) 'Optimization toolbox for use with Matlab', *User's Guide*, Natick, MA: The MathWorks, Inc., Available at: http://www.mathworks.com/access/helpdesk/help/toolbox/optim/.

Zhang, Y. and Der Kiureghian, A. (1993) 'Dynamic response sensitivity of inelastic structures', *Computer Methods in Applied Mechanics and Engineering*, Vol. 108, Nos.1/2, pp.23–36.

Zona, A., Barbato, M. and Conte, J.P. (2005) 'Finite element response sensitivity analysis of steel-concrete composite beams with deformable shear connection', *Journal of Engineering Mechanics (ASCE)*, Vol. 131, No. 11, pp.1126–1139.

Appendix

Continuity is a very desirable property of finite element response sensitivities for applications involving the use of gradient-based optimisation algorithms. Herein, a theorem giving a sufficient condition for continuity to hold is stated and proved for the case of quasi-static finite element analysis. Remarks and observations are made for the more complicated dynamic analysis case. In the sequel, the symbol $a\big|_b$ indicates that the quantity 'a' has been computed considering the quantity 'b' as a constant (i.e. b fixed), and the symbol $a\big|_{b=\bar{b}}$ indicates that the quantity 'a' is evaluated for variable 'b' equal to the value '$\bar{b}$'.

Theorem: *Given a finite element model of a structural system, the sensitivities v of the response quantities* $\mathbf{r}$ *to sensitivity parameter* θ, $v(t,\theta) = d\mathbf{r}(t,\theta)/d\theta$, *are continuous everywhere as functions of both the ordering parameter t (pseudo-time) of a quasi-static analysis and the sensitivity parameter* θ, *if the following conditions are satisfied:*

a *All the material constitutive models used for representing the structural behaviour are uniaxial constitutive laws, that is,* $\sigma = \sigma(\varepsilon)$, *in which* σ *and* ε *denote a scalar stress or stress resultant quantity and a scalar strain or strain resultant quantity, respectively.*

b *All the branches of the material constitutive models can be expanded in Taylor series about any of their points, that is,* $d^j\sigma/d\varepsilon^j\big|_{\varepsilon=\bar{\varepsilon}}$ *exists and is finite for any* $\bar{\varepsilon}$ *and* $j = 1,2,\ldots$.

c *The material constitutive models are continuously differentiable with respect to the sensitivity parameter* θ, *that is,* $\partial\sigma(\varepsilon,\theta)/\partial\theta\big|_{\varepsilon}$ *exists and is a continuous function of* θ.

d *The components of the external nodal loading vector,* $\mathbf{F}(t,\theta)$, *are continuous in terms of the ordering parameter t and continuously differentiable with respect to the sensitivity parameter* θ.

Proof: Without lack of generality, the proof will be presented for $\mathbf{r} = \mathbf{u}$, where $\mathbf{u}$ denotes the nodal displacement vector, and will refer to a single analysis step (i.e. load or displacement increment) after convergence (within a small specified tolerance) is achieved for response calculation.

For quasi-static analysis, the equilibrium equation for the space-discretised system at $t = t_{n+1}$ is expressed as

$$\mathbf{R}_{n+1}(\mathbf{u}_{n+1}(\theta),\theta) = \mathbf{F}_{n+1}(\theta) \tag{A1}$$

in which $\mathbf{R} = \mathbf{R}(\mathbf{u}(\theta),\theta)$ and $\mathbf{F}(\theta)$ denote the internal and external nodal force vectors, respectively, and where their dependence on the sensitivity parameter θ is shown explicitly; the subscript $n + 1$ indicates the load/time step number (i.e. the quantity to which it is attached is computed at $t = t_{n+1}$).

The response sensitivity equation at the structure level is obtained from Equation (34) using the chain rule of differentiation as

$$\mathbf{K}_{n+1}\frac{\mathrm{d}\mathbf{u}_{n+1}}{\mathrm{d}\theta} = \frac{\mathrm{d}\mathbf{F}_{n+1}}{\mathrm{d}\theta} - \frac{\partial\mathbf{R}_{n+1}}{\partial\theta}\bigg|_{\mathbf{u}_{n+1}} \tag{A2}$$

where **K** denotes the structure (consistent) tangent stiffness matrix. From Equation (A2), it follows that

$$\begin{cases} \dfrac{\mathrm{d}\mathbf{u}_n}{\mathrm{d}\theta} = \mathbf{K}_n^{-1}\left(\dfrac{\mathrm{d}\mathbf{F}_n}{\mathrm{d}\theta} - \left.\dfrac{\partial \mathbf{R}_n}{\partial \theta}\right|_{\mathbf{u}_n}\right) \\ \dfrac{\mathrm{d}\mathbf{u}_{n+1}}{\mathrm{d}\theta} = \mathbf{K}_{n+1}^{-1}\left(\dfrac{\mathrm{d}\mathbf{F}_{n+1}}{\mathrm{d}\theta} - \left.\dfrac{\partial \mathbf{R}_{n+1}}{\partial \theta}\right|_{\mathbf{u}_{n+1}}\right) \end{cases} \tag{A3}$$

Three different cases must be considered:

1 Continuity of response sensitivity, $\mathrm{d}\mathbf{u}/\mathrm{d}\theta$, with respect to the ordering parameter t for a load step $[t_n, t_{n+1}]$ in which the strain rate does not change sign, with θ kept fixed and equal to its nominal value θ_0.

We need to prove that

$$\lim_{t_{n+1}\to t_n}\left(\frac{\mathrm{d}\mathbf{u}_{n+1}}{\mathrm{d}\theta} - \frac{\mathrm{d}\mathbf{u}_n}{\mathrm{d}\theta}\right) = \mathbf{0} \tag{A4}$$

The assumed smoothness/continuity properties of the material constitutive models and the external loading functions (assumptions (b), (c) and (d) above) together with Equation (A1) imply that

$$\begin{cases} \lim\limits_{t_{n+1}\to t_n} \mathbf{u}_{n+1} = \mathbf{u}_n \\ \lim\limits_{t_{n+1}\to t_n} \mathbf{K}_{n+1} = \mathbf{K}_n \\ \lim\limits_{t_{n+1}\to t_n} \left.\dfrac{\partial \mathbf{R}_{n+1}}{\partial \theta}\right|_{\mathbf{u}_{n+1}} = \left.\dfrac{\partial \mathbf{R}_n}{\partial \theta}\right|_{\mathbf{u}_n} \\ \lim\limits_{t_{n+1}\to t_n} \dfrac{\mathrm{d}\mathbf{F}_{n+1}}{\mathrm{d}\theta} = \dfrac{\mathrm{d}\mathbf{F}_n}{\mathrm{d}\theta} \end{cases} \tag{A5}$$

Thus Equation (A4) is proved by substituting Equation $(A3)_{1,2}$ in its left-hand-side and using Equation $(A5)_{2,3,4}$.

2 Continuity of response sensitivity, $\mathrm{d}\mathbf{u}/\mathrm{d}\theta$, with respect to ordering parameter t for a load step $[t_n, t_{n+1}]$ in which the strain rate changes sign (i.e. t_n corresponds exactly to an unloading point), with θ kept fixed and equal to its nominal value θ_0.

We need to prove Equation (A4) again. In this subcase, Equation $(A5)_2$ is not satisfied as, in general, $\lim\limits_{t_{n+1}\to t_n} \mathbf{K}_{n+1} = \mathbf{K}_{n,\text{unloading}} \neq \mathbf{K}_{n,\text{loading}}$ (see Figure 6(b)). The internal and external nodal force vectors at $t = t_{n+1}$ can be written in incremental form as

$$\begin{cases} \mathbf{R}_{n+1} = \mathbf{R}_n + \Delta\mathbf{R}_{n+1} \\ \mathbf{F}_{n+1} = \mathbf{F}_n + \Delta\mathbf{F}_{n+1} \end{cases} \tag{A6}$$

Equilibrium as expressed in Equation (A1) requires also that

$$\begin{cases} \mathbf{R}_n = \mathbf{F}_n \\ \Delta\mathbf{R}_{n+1} = \Delta\mathbf{F}_{n+1} \end{cases} \tag{A7}$$

Taylor series expansion of the internal nodal force vector $\mathbf{R}$ (considered as function of the nodal displacement vector $\mathbf{u}$) about $\mathbf{u} = \mathbf{u}_{n+1}$ is expressed at $\mathbf{u} = \mathbf{u}_n$ as

$$\mathbf{R}(\mathbf{u}_n) = \mathbf{R}(\mathbf{u}_{n+1}) + \sum_{p=1}^{\infty} \frac{1}{p!} \left\{ \left[\left(\mathbf{u}_n - \mathbf{u}_{n+1} \right)^{\mathrm{T}} \nabla_{\mathbf{u}} \right]^p \mathbf{R}(\mathbf{u}) \right\} \Big|_{\mathbf{u}=\mathbf{u}_{n+1}} \tag{A8}$$

in which $\nabla_{\mathbf{u}} = [(\partial / \partial u_1) \cdots (\partial / \partial u_N)]^T$, N denotes the number of degrees of freedom of the system, and the superscript T represents the vector/matrix transpose operator. Considering that $\mathbf{R}(\mathbf{u}_n) = \mathbf{R}_n$ and $\mathbf{R}(\mathbf{u}_{n+1}) = \mathbf{R}_{n+1}$, we can also write

$$\mathbf{R}_{n+1} = \mathbf{R}_n - \sum_{p=1}^{\infty} \frac{(-1)^p}{p!} \left\{ \left[\left(\mathbf{u}_{n+1} - \mathbf{u}_n \right)^{\mathrm{T}} \nabla_{\mathbf{u}} \right]^p \mathbf{R}(\mathbf{u}) \right\} \Big|_{\mathbf{u}=\mathbf{u}_{n+1}} \tag{A9}$$

Differentiating Equation (A9) with respect to parameter θ at $\theta = \theta_0$, and recognising that $\partial / \partial\theta (\partial \mathbf{R}(\mathbf{u}) / \partial u_i \,|_{\mathbf{u}=\mathbf{u}_{n+1}}) = \mathbf{0}$, $i = 1, \ldots, N$ (since $\partial \mathbf{R}(\mathbf{u}) / \partial u_i$ depends on θ only implicity through $\mathbf{u}(\theta)$ and the operation $(\cdots)|_{\mathbf{u}=\mathbf{u}_{n+1}}$ removes any dependence on θ since $\mathbf{u}_{n+1}$ has been computed for $\theta = \theta_0$), we obtain

$$\frac{\mathrm{d}\mathbf{R}_{n+1}}{\mathrm{d}\theta} = \frac{\mathrm{d}\mathbf{R}_n}{\mathrm{d}\theta} + \sum_{p=1}^{\infty} \frac{(-1)^{p+1}}{(p-1)!} \left\{ \left\{ \left[\left(\mathbf{u}_{n+1} - \mathbf{u}_n \right)^T \nabla_{\mathbf{u}} \right]^{p-1} \left(\frac{\mathrm{d}\mathbf{u}_{n+1}}{\mathrm{d}\theta} - \frac{\mathrm{d}\mathbf{u}_n}{\mathrm{d}\theta} \right)^T \nabla_{\mathbf{u}} \right\} \mathbf{R}(\mathbf{u}) \right\} \Big|_{\mathbf{u}=\mathbf{u}_{n+1}} \tag{A10}$$

From Equation (A10), we obtain the conditional derivative $\partial \mathbf{R}_{n+1} / \partial\theta \,|_{\mathbf{u}_{n+1}}$ as

$$\left. \frac{\partial \mathbf{R}_{n+1}}{\partial \theta} \right|_{\mathbf{u}_{n+1}} = \frac{d\mathbf{R}_n}{d\theta} + \sum_{p=1}^{\infty} \frac{(-1)^p}{(p-1)!} \left\{ \left\{ \left[\left(\mathbf{u}_{n+1} - \mathbf{u}_n \right)^{\mathrm{T}} \nabla_{\mathbf{u}} \right]^{p-1} \left(\frac{\mathrm{d}\mathbf{u}_n}{\mathrm{d}\theta} \right)^{\mathrm{T}} \nabla_{\mathbf{u}} \right\} \mathbf{R}(\mathbf{u}) \right\} \Big|_{\mathbf{u}=\mathbf{u}_{n+1}} \tag{A11}$$

recognising that $\partial \mathbf{R}_n / \partial\theta \,|_{\mathbf{u}_{n+1}} = \mathrm{d}\mathbf{R}_n / \mathrm{d}\theta$ (since $\mathrm{d}\mathbf{R}_n / \mathrm{d}\theta$ is independent of the response $\mathbf{u}_{n+1}$ computed at a subsequent analysis step) and $\partial \mathbf{u}_{n+1} / \partial\theta \,|_{\mathbf{u}_{n+1}} = \mathbf{0}$. For $\mathbf{u}_{n+1}$ sufficiently close to $\mathbf{u}_n$, the terms in Equation (A11) that are multiplied by $(u_{i,n+1} - u_{i,n})^j$ ($i = 1, \ldots, N; j \geq 1$) are negligibly small (i.e. infinitesimal quantities) due to assumption (b) which implies that the quantities $\partial^j \mathbf{R}(\mathbf{u}) / \partial u_1^{j_1} \ldots \partial u_N^{j_N} \,|_{\mathbf{u}=\mathbf{u}_{n+1}}$ ($j = 1, 2,$ ... and $\sum_{k=1}^{N} j_k = j$) exist and are finite. Thus, discarding infinitesimal quantities in Equation (A11), we obtain that

$$\lim_{\mathbf{u}_{n+1} \to \mathbf{u}_n} \left. \frac{\partial \mathbf{R}_{n+1}}{\partial \theta} \right|_{\mathbf{u}_{n+1}} = \frac{\mathrm{d}\mathbf{R}_n}{\mathrm{d}\theta} - \left\{ \left[\left(\frac{\mathrm{d}\mathbf{u}_n}{\mathrm{d}\theta} \right)^T \nabla_{\mathbf{u}} \right] \mathbf{R}(\mathbf{u}) \right\} \Big|_{\mathbf{u}=\mathbf{u}_{n+1}} = \frac{\mathrm{d}\mathbf{R}_n}{\mathrm{d}\theta} - \mathbf{K}_{n+1} \frac{\mathrm{d}\mathbf{u}_n}{\mathrm{d}\theta} \tag{A12}$$

in which the equivalence between consistent tangent moduli and continuum tangent moduli for uniaxial material constitutive models is used (assumption (a); Simo and Hughes, 1998; Conte et al., 2003). Finally, substituting Equation $(A3)_2$ in Equation (A4) and making use of Equations (A11), $(A5)_1$ and (A12) (in this order), we obtain

$$\begin{aligned}\lim_{t_{n+1}\to t_n}\left(\frac{\mathrm{d}\mathbf{u}_{n+1}}{\mathrm{d}\theta}-\frac{\mathrm{d}\mathbf{u}_n}{\mathrm{d}\theta}\right) &= \lim_{t_{n+1}\to t_n}\left[\mathbf{K}_{n+1}^{-1}\left(\frac{\mathrm{d}\mathbf{F}_{n+1}}{d\theta}-\left.\frac{\partial\mathbf{R}_{n+1}}{\partial\theta}\right|_{\mathbf{u}_{n+1}}\right)-\frac{\mathrm{d}\mathbf{u}_n}{\mathrm{d}\theta}\right] \\ &= \lim_{t_{n+1}\to t_n}\left[\mathbf{K}_{n+1}^{-1}\left(\frac{\mathrm{d}\mathbf{F}_{n+1}}{\mathrm{d}\theta}-\frac{\mathrm{d}\mathbf{R}_n}{\mathrm{d}\theta}\right)+\frac{\mathrm{d}\mathbf{u}_n}{\mathrm{d}\theta}-\frac{\mathrm{d}\mathbf{u}_n}{\mathrm{d}\theta}\right]=\mathbf{0}\end{aligned} \tag{A13}$$

in which we used the relation

$$\lim_{t_{n+1}\to t_n}\frac{\mathrm{d}\mathbf{F}_{n+1}}{\mathrm{d}\theta}=\frac{\mathrm{d}\mathbf{F}_n}{\mathrm{d}\theta}=\frac{\mathrm{d}\mathbf{R}_n}{\mathrm{d}\theta}$$

obtained by differentiating Equation $(A7)_1$ and combining the result with Equation $(A5)_4$.

3 Continuity of response sensitivity, $\mathrm{d}\mathbf{u}/\mathrm{d}\theta$, with respect to sensitivity parameter θ (for $t = t_{n+1}$ fixed).

Let us consider a perturbed value $\tilde{\theta}$ of the sensitivity parameter, that is, $\tilde{\theta} = \theta_0 + \Delta\theta$, in which θ_0 denotes the nominal value of the parameter and $\Delta\theta$ is a small but finite perturbation of it. Let $\boldsymbol{f} = \boldsymbol{f}(t,\theta)$ denote a response or response sensitivity vector quantity as function of both the ordering parameter t and sensitivity parameter θ and let $\mathbf{f} = \boldsymbol{f}(t,\theta)\big|_{\theta=\theta_0}$ and $\tilde{\mathbf{f}} = \boldsymbol{f}(t,\theta)\big|_{\theta=\tilde{\theta}}$, respectively. We need to prove that

$$\lim_{\tilde{\theta}\to\theta_0}\left(\frac{\mathrm{d}\tilde{\mathbf{u}}_{n+1}}{\mathrm{d}\theta}-\frac{\mathrm{d}\mathbf{u}_{n+1}}{\mathrm{d}\theta}\right)=\lim_{\Delta\theta\to 0}\left(\frac{\mathrm{d}\tilde{\mathbf{u}}_{n+1}}{\mathrm{d}\theta}-\frac{\mathrm{d}\mathbf{u}_{n+1}}{\mathrm{d}\theta}\right)=\mathbf{0} \tag{A14}$$

From the continuity of the response and the loading function(s) with respect to the sensitivity parameter θ (assumptions (c) and (d)), it follows that

$$\begin{cases}\lim_{\Delta\theta\to 0}\tilde{\mathbf{u}}_{n+1}=\mathbf{u}_{n+1}\\ \lim_{\Delta\theta\to 0}\tilde{\mathbf{K}}_{n+1}=\mathbf{K}_{n+1}\\ \lim_{\Delta\theta\to 0}\tilde{\mathbf{R}}_{n+1}=\mathbf{R}_{n+1}\\ \lim_{\Delta\theta\to 0}\tilde{\mathbf{F}}_{n+1}=\mathbf{F}_{n+1}\end{cases} \tag{A15}$$

Making use of the static equilibrium Equation (A1) and assumption (d), we have

$$\lim_{\Delta\theta\to 0}\frac{\mathrm{d}\tilde{\mathbf{R}}_{n+1}}{\mathrm{d}\theta}=\lim_{\Delta\theta\to 0}\frac{\mathrm{d}\tilde{\mathbf{F}}_{n+1}}{\mathrm{d}\theta}=\frac{\mathrm{d}\mathbf{F}_{n+1}}{\mathrm{d}\theta}=\frac{\mathrm{d}\mathbf{R}_{n+1}}{\mathrm{d}\theta} \tag{A16}$$

From the chain rule of differentiation applied to the internal force vector $\mathbf{R}$ expressed as function of parameter θ (i.e. $\mathbf{R} = \mathbf{R}(\mathbf{u}(\theta),\theta)$), we also have

$$\begin{cases} \dfrac{\mathrm{d}\tilde{\mathbf{R}}_{n+1}}{\mathrm{d}\theta} = \tilde{\mathbf{K}}_{n+1}\dfrac{\mathrm{d}\tilde{\mathbf{u}}_{n+1}}{\mathrm{d}\theta} + \left.\dfrac{\partial\tilde{\mathbf{R}}_{n+1}}{\partial\theta}\right|_{\tilde{\mathbf{u}}_{n+1}} \\ \dfrac{\mathrm{d}\mathbf{R}_{n+1}}{\mathrm{d}\theta} = \mathbf{K}_{n+1}\dfrac{\mathrm{d}\mathbf{u}_{n+1}}{\mathrm{d}\theta} + \left.\dfrac{\partial\mathbf{R}_{n+1}}{\partial\theta}\right|_{\mathbf{u}_{n+1}} \end{cases} \tag{A17}$$

Furthermore, from assumption (c), it follows that $\lim_{\Delta\theta\to 0} \partial\tilde{\mathbf{R}}/\partial\theta\,|_{\mathbf{u}} = \partial\mathbf{R}/\partial\theta\,|_{\mathbf{u}}$, which when combined with Equation (A15)$_1$ gives

$$\lim_{\Delta\theta\to 0} \left.\frac{\partial\tilde{\mathbf{R}}_{n+1}}{\partial\theta}\right|_{\tilde{\mathbf{u}}_{n+1}} = \left.\frac{\partial\mathbf{R}_{n+1}}{\partial\theta}\right|_{\mathbf{u}_{n+1}} \tag{A18}$$

From Equation (A17) and using Equations (A16), (A15)$_2$ and (A18), it follows that

$$\lim_{\Delta\theta\to 0} \frac{d\tilde{\mathbf{u}}_{n+1}}{d\theta} = \frac{d\mathbf{u}_{n+1}}{d\theta} \tag{A19}$$

Remarks on the sufficient conditions for response sensitivity continuity

The sufficient conditions required by the above theorem are easy to satisfy. In particular, condition (b) (requiring that all branches of the material constitutive models used be expandable in Taylor series) is in general satisfied by common smooth material models, provided that branches with infinite stiffness are avoided.

The only condition that actually restricts the application of the above theorem is condition (a) (all material constitutive models need to be uniaxial), which is required by Equation (A12), where the identity between continuum and consistent tangent moduli for uniaxial constitutive models is used. Other researchers (Haukaas and Der Kiureghian, 2004) found that continuity of finite element response sensitivities can be obtained by using smooth multiaxial constitutive models. Thus, it appears that the above theorem may be extendable to multiaxial material constitutive models.

Remarks and observations for the dynamic analysis case

The proof of the above theorem for quasi-static analysis cannot be easily extended to the case of dynamic analysis. The space and time discretised equations of motion of a structural system subjected to dynamic loads can be written as

$$\left[a_1\mathbf{M}(\theta)\mathbf{u}_{n+1}(\theta) + a_5\mathbf{C}(\theta)\mathbf{u}_{n+1}(\theta) + \mathbf{R}_{n+1}(\mathbf{u}_{n+1}(\theta),\theta)\right] = \bar{\mathbf{F}}_{n+1}(\theta) \tag{A20}$$

in which

$$\begin{aligned} \bar{\mathbf{F}}_{n+1}(\theta) = \mathbf{F}_{n+1}(\theta) &- \mathbf{M}(\theta)\left(a_2\mathbf{u}_n(\theta) + a_3\dot{\mathbf{u}}_n(\theta) + a_4\ddot{\mathbf{u}}_n(\theta)\right) \\ &- \mathbf{C}(\theta)\left(a_6\mathbf{u}_n(\theta) + a_7\dot{\mathbf{u}}_n(\theta) + a_8\ddot{\mathbf{u}}_n(\theta)\right) \end{aligned} \tag{A21}$$

and the following general one-step time integration scheme is used (Conte et al., 1995; Conte 2001; Conte et al., 2003, 2004; Haukaas and Der Kiureghian, 2004; Barbato and Conte, 2005)

$$\begin{cases} \ddot{\mathbf{u}}_{n+1} = a_1 \mathbf{u}_{n+1} + a_2 \mathbf{u}_n + a_3 \dot{\mathbf{u}}_n + a_4 \ddot{\mathbf{u}}_n \\ \dot{\mathbf{u}}_{n+1} = a_5 \mathbf{u}_{n+1} + a_6 \mathbf{u}_n + a_7 \dot{\mathbf{u}}_n + a_8 \ddot{\mathbf{u}}_n \end{cases} \tag{A22}$$

The above family of time stepping schemes includes well-known algorithms such as the Newmark-beta family of methods (e.g. constant average acceleration method, linear acceleration method, Fox-Goodwin method, central difference method) and the Wilson-theta method (Hughes, 1987).

Differentiating Equation (A20) with respect to the sensitivity parameter θ yields the following sensitivity equation:

$$\mathbf{K}_{n+1}^{dyn} \frac{\mathrm{d}\mathbf{u}_{n+1}}{\mathrm{d}\theta} = \left(\frac{\mathrm{d}\mathbf{F}}{\mathrm{d}\theta} \right)_{n+1}^{dyn} - \left. \frac{\partial \mathbf{R}_{n+1}}{\partial \theta} \right|_{\mathbf{u}_{n+1}} \tag{A23}$$

in which the terms $(d\mathbf{F}/d\theta)_{n+1}^{dyn}$ and $\mathbf{K}_{n+1}^{dyn}$ are defined as

$$\begin{aligned} \left(\frac{d\mathbf{F}}{d\theta} \right)_{n+1}^{dyn} &= \frac{\mathrm{d}\mathbf{F}_{n+1}}{\mathrm{d}\theta} - \frac{\mathrm{d}\mathbf{M}}{\mathrm{d}\theta} \left(a_1 \mathbf{u}_{n+1} + a_2 \mathbf{u}_n + a_3 \dot{\mathbf{u}}_n + a_4 \ddot{\mathbf{u}}_n \right) - \mathbf{M} \left(a_2 \frac{\mathrm{d}\mathbf{u}_n}{\mathrm{d}\theta} + a_3 \frac{\mathrm{d}\dot{\mathbf{u}}_n}{\mathrm{d}\theta} + a_4 \frac{\mathrm{d}\ddot{\mathbf{u}}_n}{\mathrm{d}\theta} \right) \\ &\quad - \frac{\mathrm{d}\mathbf{C}}{\mathrm{d}\theta} \left(a_5 \mathbf{u}_{n+1} + a_6 \mathbf{u}_n + a_7 \dot{\mathbf{u}}_n + a_8 \ddot{\mathbf{u}}_n \right) - \mathbf{C} \left(a_6 \frac{\mathrm{d}\mathbf{u}_n}{\mathrm{d}\theta} + a_7 \frac{\mathrm{d}\dot{\mathbf{u}}_n}{\mathrm{d}\theta} + a_8 \frac{\mathrm{d}\dot{\mathbf{u}}_n}{\mathrm{d}\theta} \right) \\ &= \frac{\mathrm{d}\bar{\mathbf{F}}_{n+1}}{\mathrm{d}\theta} - \left(a_1 \frac{\mathrm{d}\mathbf{M}}{\mathrm{d}\theta} + a_5 \frac{\mathrm{d}\mathbf{C}}{\mathrm{d}\theta} \right) \mathbf{u}_{n+1} \end{aligned} \tag{A24}$$

$$\mathbf{K}_{n+1}^{dyn} = a_1 \mathbf{M} + a_5 \mathbf{C} + \mathbf{K}_{n+1} \tag{A25}$$

Equation (A23) is formally identical to Equation (A2). Therefore, if we assume (in addition to the hypotheses of the theorem presented above) that:

1 the mass matrix, **M**, and the damping matrix, **C**, are time-invariant and

2 the term $\left(\mathrm{d}\mathbf{F}/\mathrm{d}\theta \right)_{n+1}^{dyn}$ is continuous as a function of θ,

we could prove the continuity of the response sensitivities $\mathrm{d}\mathbf{u}/\mathrm{d}\theta$, $\mathrm{d}\dot{\mathbf{u}}/\mathrm{d}\theta$, and $\mathrm{d}\ddot{\mathbf{u}}/\mathrm{d}\theta$ in a way that is similar to the one used for the quasi-static case.

Unfortunately, while assumption (1) is generally satisfied for civil structures (i.e. inertial properties remain usually constant within a dynamic load event, and damping properties are typically modelled through a time-invariant viscous damping mechanism), it was found through application examples such as the one shown in Figure 15 that assumption (2) is not true in general.

Assuming the same smoothness hypotheses (i.e. assumptions (b), (c) and (d)) used in the above theorem for quasi-static problems, intuition would suggest that response sensitivities are also continuous in the dynamic case that further benefits from the 'linearisation' (and smoothing) effects of the linear inertial and damping terms (Haukaas and Der Kiureghian, 2004). The fact that discontinuities are hard to detect in response

sensitivity histories (i.e. along the time axis for θ fixed), as illustrated by Figures 8 and 9, further reinforces this intuitive argument. However, finite element response sensitivities computed from the space and time discretised equations of motion, Equation (A20), and the corresponding sensitivity equations, Equation (A23), are not continuous in general. This statement is clearly illustrated in Figure 15 which clearly shows, for the example structure presented in this paper and modelled using the smooth M–P (R_0 = 20) material constitutive law, discontinuities in the response sensitivities along the parameter (F_{y0}) axis, even though discontinuities cannot be visually observed along the time axis (for a given value of F_{y0}). Discontinuities in the response sensitivities along the parameter axes are of highest interest, as they can have detrimental effects on the convergence of gradient-based optimisation algorithms such as the ones used for the design point search in structural reliability analysis (see Section 4.3).

Analytical treatment of the observed discontinuities along the parameter axes for the dynamic analysis case and for a smooth material constitutive model (such as the M–P model) is very challenging and is outside the scope of this paper. There are some fundamental differences between the quasi-static case (treated in the above theorem) and the dynamic case discussed here. By comparing the response sensitivity equations for the quasi-static case, Equation (A2) and the dynamic case, Equation (A23), we notice the following two significant changes.

a In the dynamic case, the term $(\mathrm{d}\mathbf{F}/\mathrm{d}\theta)_{n+1}^{dyn}$ on the right-hand-side of the sensitivity Equation (A23) depends on both the response and response sensitivity histories up to the current time step as shown in Equation (A24), which is not the case for the corresponding term $\mathrm{d}\mathbf{F}_{n+1}/\mathrm{d}\theta$ on the righ-hand-side of the sensitivity Equation (A2) for the quasi-static case.

b The term $(\mathrm{d}\mathbf{F}/\mathrm{d}\theta)_{n+1}^{dyn}$ and the dynamic tangent stiffness matrix, $\mathbf{K}_{n+1}^{dyn}$, depend explicitly on the time step length Δt as shown by Equations (A24) and (A25).

Indeed, the time stepping algorithm in Equation (A22) assumes a finite (and fixed) Δt and coefficients a_i (i = 1,…, 8) are, in general, dependent on Δt, that is, $a_i = a_i(\Delta t)$ (i = 1,…, 8). For example, if the Newmark-beta algorithm is used, we have $a_1 = 1\Big/\Big[\beta(\Delta t)^2\Big] = -a_2$, $a_3 = -1\big/(\beta\Delta t)$, $a_4 = 1 - 1\big/(2\beta)$, $a_5 = \alpha\big/(\beta\Delta t) = -a_6$, $a_7 = 1 - \alpha/\beta$, $a_8 = \big[1 - \alpha\big/(2\beta)\big]\Delta t$, in which α and β are parameters controlling the accuracy and stability of the numerical integration scheme (for the constant average acceleration method used in this paper, $\alpha = 1/2$ and $\beta = 1/4$)."

$$\lim_{\Delta\theta\to 0}\left(\left.\frac{\mathrm{d}\tilde{\mathbf{u}}_{n+1}}{\mathrm{d}\theta}\right|_{\Delta t}\right) \neq \left.\frac{\mathrm{d}\mathbf{u}_{n+1}}{\mathrm{d}\theta}\right|_{\Delta t} \tag{A26}$$

Convergence studies of response sensitivities suggest that such discontinuities expressed in Equation (A26) tend to spread (reduce in size and increase in number) for decreasing Δt. A comparison between the results presented in Figure 15 (large discontinuities) and the results shown in Figure 13 (small discontinuities, not visible at the given scale) shows clearly the effect of reducing the time step length Δt from 0.02sec to 0.001sec upon the computed response sensitivities for the smooth M–P (R_0 = 20) material constitutive law.

On the basis of the application examples performed, it can be safely concluded that the response sensitivity discontinuities shown in Figure 15 are largely due to the discretisation in time of the equations of motion, Equation (A20). The solution of the time-continuous problem for smooth material constitutive models (satisfying the hypotheses of the theorem presented above) appears to have continuous response sensitivities, as suggested by intuition, that is,

$$\lim_{\Delta\theta\to 0}\left[\lim_{\Delta t\to 0}\left(\frac{\mathrm{d}\tilde{\mathbf{u}}_{n+1}}{\mathrm{d}\theta}\right)\right]=\lim_{\Delta t\to 0}\left(\frac{\mathrm{d}\mathbf{u}_{n+1}}{\mathrm{d}\theta}\right) \tag{A27}$$

For practical purposes and finite element applications, the result expressed by Equation (A27) requires a fine time discretisation in integrating the equation of motion to obtain continuous (and therefore converged with respect to Δt) response sensitivities (see Figure 13 for converged results and Figure 15 for non-converged results). Previous studies show that convergence requirements (with respect to Δt) for response sensitivity computation are stricter than those for response computation only (Gu and Conte, 2003). It is noteworthy that non-smooth material constitutive models (such as the J_2 plasticity model considered in this paper) present discontinuities along the parameter axes that are due to the physics of the problem (material state transition from elastic to plastic at integration point(s)), and thus cannot be eliminated through reducing Δt (see Figure 14).